*Smart Antennas.* Tapan K. Sarkar, Michael C. Wicks,
Magdalena Salazar-Palma, Robert J. Bonneau

ISBN: 0-471-21010-2

# 8

# A SURVEY OF VARIOUS PROPAGATION MODELS FOR MOBILE COMMUNICATION

## SUMMARY

For mobile systems, in order to estimate the signal parameters accurately, it is necessary to estimate its propagation characteristics through a medium. The propagation analysis provides a good initial estimate of the signal characteristics. The ability to accurately predict radio propagation behavior for wireless personal communication systems such as cellular mobile radio is becoming crucial to system design. Since site measurements are costly, propagation models have been developed as a suitable low-cost, convenient alternative. Channel modeling is required to predict path loss and to characterize the impulse response of the propagating channel. The path loss is associated with the design of base stations, as this tells us how much a transmitter should need to radiate to service a given region. Channel characterization, on the other hand, deals with the fidelity of the received signals and has to do with the nature of the waveform received at a receiver. The objective here is to design a suitable receiver that will receive the distorted transmitted signal due to the multipath and dispersion effects of the channel and decode the transmitted signal. An understanding of the various propagation models can actually address both problems. This chapter begins with a review of the available information provided by the various propagation models for both indoor and outdoor environments. The existing models can be classified into two major classes: statistical models and site-specific models. The main characteristics of a radio channel, such as path loss, fading, and time delay spread, are discussed. Currently, a third alternative, which includes many new numerical methods, is being introduced into propagation prediction. The advantages and disadvantages of some of these methods are summarized. In addition, an impulse response characterization for the propagation path is presented, including models for small-scale fading.

## 8.1 INTRODUCTION

The commercial success of cellular communications since its initial implementation in the early 1980s has led to an intense interest among wireless engineers in understanding and predicting radio propagation characteristics in various urban and suburban areas, even within buildings. As the explosive growth of mobile communications continues, it is very valuable to have the capability of determining optimum base station locations, obtaining a suitable data rate, and estimating their coverage without conducting a series of propagation measurements, which are very expensive and time consuming. In order to provide design guidelines and installations of the mobile systems, it is therefore important to develop effective propagation models for mobile communication.

## 8.2 DEFINITIONS AND TERMINOLOGIES USED FOR CHARACTERIZING VARIOUS PARAMETERS OF A PROPAGATION CHANNEL

In order to understand the nature of the models that are going to be presented, several definitions and terminologies for both narrowband and wideband wave propagation over a radio channel are first described to make the reader familiar with the terminologies and parameters of the problem.

### 8.2.1 Path Loss

Path loss (PL) is a measure of the average RF attenuation suffered by a transmitted signal when it arrives at the receiver after traversing several wavelengths. It is defined by [1]

$$\text{PL(dB)} = 10 \log \frac{P_t}{P_r} \tag{8.1}$$

where $P_t$ and $P_r$ are the transmitted and received power, respectively. In free space, power reaching the receiving antenna, which is separated from the transmitting antenna by a distance $d$, is given by the Friis free-space equation:

$$P_r(d) = \frac{P_t G_t G_r \lambda^2}{(4\pi)^2 d^2 L} \tag{8.2}$$

where $G_t$ and $G_r$ are the gain of the transmitting and receiving antenna, respectively, $L$ is the system loss factor not related to propagation, and $\lambda$ is the wavelength in meters. It is clear that equation (8.2) does not hold for $d = 0$.

Hence, many propagation models use a different representation for a close-in distance, $d_0$, known as the received power reference point. It is typically chosen to be 1 m. In realistic mobile radio channels, free space is not the appropriate propagation medium. A general PL model uses a parameter, $\gamma$, to denote the power law relationship between the separation distance and the received power. So path loss (in decibels) can be expressed as [2]

$$\mathrm{PL}(d) = \mathrm{PL}(d_0) + 10\gamma \log(d/d_0) + X_\sigma \tag{8.3}$$

where $\gamma = 2$ characterizes free space. However, it is generally higher for wireless channels. $X_\sigma$ denotes a zero mean Gaussian random variable of standard deviation $\sigma$ that reflects the variation on the average of the received power that naturally occurs when a PL model of this type is used. Path loss is the main ingredient of a propagation model. It is related to the area of coverage of mobile systems.

### 8.2.2 Power Delay Profile

The random and complicated radio propagation channels can be characterized using the impulse response approach. For each point in the three-dimensional environment, the channel is a linear filter with the impulse response $h(t)$. The impulse response provides a wideband characterization of the propagating channel and contains all the information necessary to simulate or analyze any type of radio transmission through that channel.

Multipath propagation causes severe dispersion of the transmitted signal. The expected degree of dispersion is determined through measurement of the power delay profile of the channel. The power delay profile provides an indication of the dispersion or distribution of transmitted power over various paths in a multipath model for propagation. The power delay profile of the channel is calculated by taking the spatial average of $|h(t)|^2$ over a local area. By making several local area measurements of $|h(t)|^2$ for different locations, it is possible to build an ensemble of power delay profiles, each representing a possible small-scale multipath channel state [3, 10]. A typical plot of the power delay profile is shown in Figure 8.1.

Many multipath channel parameters are derived from the power delay profile. Power delay profiles are measured using wideband channel sounding techniques and are presented in the form of plots of the received power as a function of an additional or excess delay with respect to a fixed time delay reference. There is a delay between when the signal is transmitted to the time when it is received, due to the finite velocity of propagation of the electromagnetic signal. However, additional delay may be introduced by the propagation medium as well. A mobile channel exhibits a continuous multipath structure, hence the power delay profile can be thought of as a density function of the form

$$P(\tau) = \frac{|h(t)|^2}{\int_{-\infty}^{\infty} |h(t)|^2 \, dt} \tag{8.4}$$

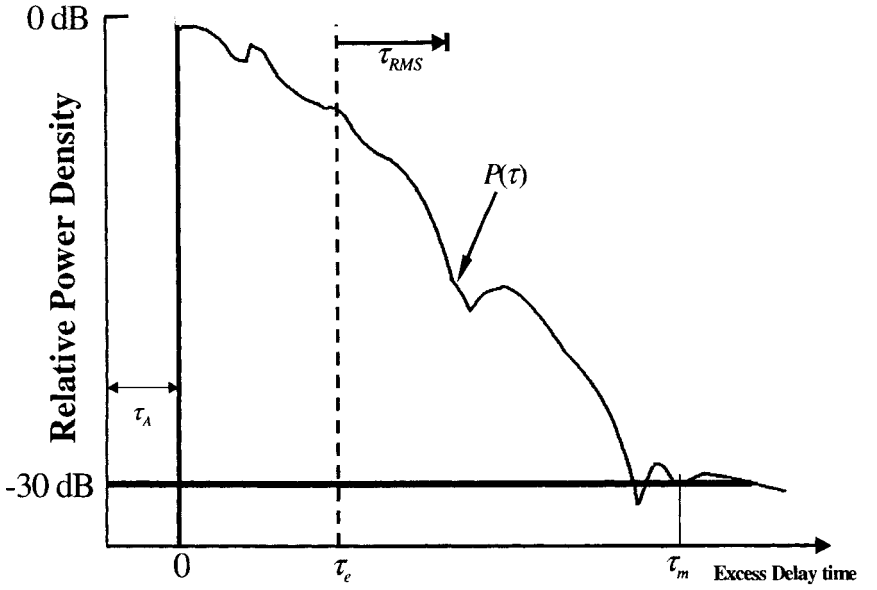


**Figure 8.1.** Typical power delay profile and definition of the delay parameters.

### 8.2.3 Time Delay Spread

Time dispersion varies widely in a mobile radio channel, due to the fact that reflections and scattering occur at seemingly random locations, and the resulting multipath channel response appears random as well. Because time dispersion is dependent on the geometric positional relationships between the transmitter, receiver, and the surrounding physical environment, some parameters, which can grossly quantify the multipath channel, are used. They are as follows.

*8.2.3.1 First Arrival Delay* ($\tau_A$). This time delay corresponds to the arrival of the first transmitted signal at the receiver. It is usually measured at the receiver. This delay is set by the minimum possible propagation path delay from the transmitter to the receiver. It serves as a reference, and all delay measurements are taken relative to it. How the origin is defined is shown in Figure 8.1. Any delay measured longer than this reference delay is called an *excess delay*.

*8.2.3.2 Mean Excess Delay* ($\tau_e$). This is the first moment of the power delay profile, as shown in Figure 8.1 with respect to the first delay and is expressed as

$$\tau_e = \int (\tau - \tau_A) P(\tau) d\tau \tag{8.5}$$

*8.2.3.3 RMS Delay* ($\tau_{\text{RMS}}$). This is the square root of the second central moment of a power delay profile, as seen in Figure 8.1. It is the standard deviation about the mean excess delay and is expressed as

$$\tau_{\text{RMS}} = [\int (\tau - \tau_e - \tau_A)^2 P(\tau) d\tau]^{1/2} \tag{8.6}$$

RMS delay is a good measure of the multipath spread. It gives an indication of the nature of the intersymbol interference (ISI). Strong echoes (relative to the shortest path) with long delays contribute significantly to $\tau_{\text{RMS}}$. The effects of dispersion on the performance of a digital receiver can be related reliably only to the RMS delay, independent of the shape of the power-delay profile, so long as it is small compared to the symbol period ($T$) of the digital modulation. It is also used to give an estimate of the maximum data rate of transmission.

*8.2.3.4 Maximum Excess Delay* ($\tau_m$). This is measured with respect to a specific power level which is characterized as the threshold of the signal. When the signal level is lower than the threshold, it is processed as noise. For example, in Figure 8.1 the maximum excess delay spread can be specified as the excess delay ($\tau_m$) for which $P(\tau)$ falls below −30 dB of its peak value, as shown in Figure 8.1.

### 8.2.4 Coherence Bandwidth

Whereas the delay spread is a natural phenomenon caused by reflection and scattering of the transmitted signal in a radio channel, the coherence bandwidth, $B_C$, is defined in terms of the RMS delay spread. It is a statistical measure of the range of frequencies over which the channel can be considered "flat ." It is defined as the bandwidth over which the variation of the signal is about 10% and is approximated by [4, 10]

$$B_C \approx \frac{1}{50\,\tau_{\text{RMS}}} \tag{8.7}$$

It is important to note that an exact relationship between the coherence bandwidth and the RMS delay spread does not exist. The real coherence bandwidth depends on the actual impulse response of the channel.

### 8.2.5 Types of Fading

The type of fading experienced by a signal propagating through a mobile radio channel depends on the nature of the transmitted signal as well as on the characteristics of the channel. Different transmitted signals will undergo different types of fading according to the relation between the signal parameters, [such as path loss, bandwidth (BW), symbol period, etc.] and the channel parameters (such as RMS delay spread and Doppler spread). Figure 8.2 describes the different types of fading and the different relationships that exist between them [5].

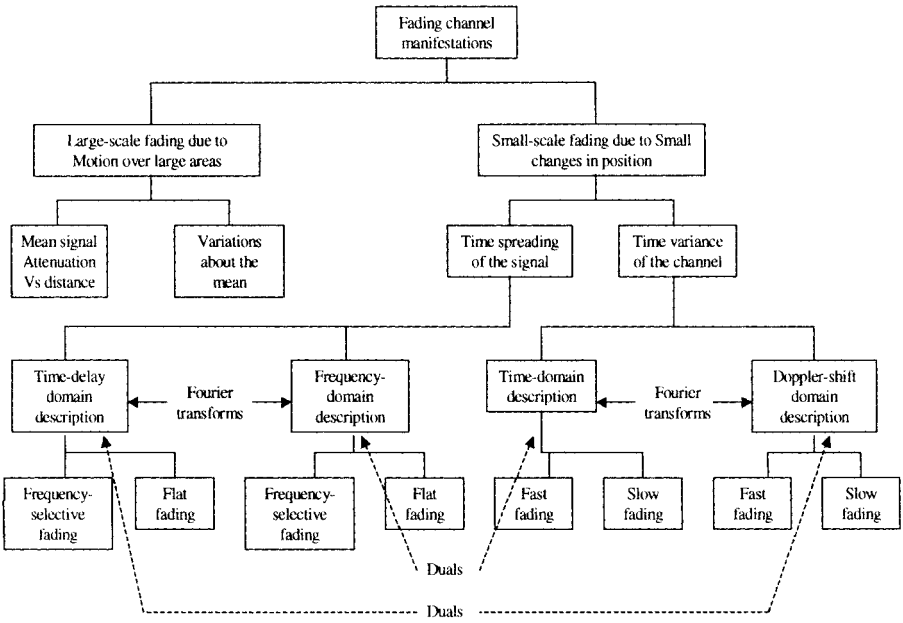


**Figure 8.2.** Types of fading.

The phenomenon of large-scale fading is affected primarily by the presence of hills, forests, and buildings between the transmitter and the receiver. The statistics of large-scale fading provide a way of computing an estimate of the path loss as a function of distance and other factors.

A channel is said to exhibit frequency-selective fading when the delay spread is greater than the symbol period. This condition occurs whenever the received multipath components of a symbol extend beyond the time duration of the symbols. Such multipath dispersion of the signal yields a kind of inter-symbol interference (ISI) called *channel-induced ISI*. When the delay spread is

less than the symbol period, a channel is said to exhibit *flat fading* and there is no channel-induced ISI distortion. But there can still be performance degradation due to the irresolvable phasor components that add up destructively to yield a substantial reduction in signal-to-noise ratio (SNR) at the receiver.

Fast fading and slow fading are classified on the basis of how rapidly transmitted baseband signal changes as compared to the rate of electrical parameter changes of the channel. If the channel impulse response changes at a rate much faster than the transmitted signal, the channel may be assumed to be a fast-fading channel. Otherwise, it is assumed to be a slow-fading channel. It is important to note that the velocity of the mobile or velocity of objects using the channel through a baseband signal determines whether a signal undergoes fast or slow fading.

### 8.2.6 Adaptive Antenna

An application of antenna arrays has been suggested in recent years for mobile communications systems to overcome the problems of single-antenna systems. The use of adaptive antenna arrays helps in improving the system performance by increasing channel capacity and spectrum efficiency, extending range coverage, tailoring beam shape, steering multiple beams to track many mobiles, and compensating for the aperture distortion electronically. It also reduces multipath fading, co-channel interferences, system complexity and cost, bit error rate (BER), and outage probability [6].

A phased array antenna uses an array of simple antennas and combines the signal induced on the elements to form the output. The term *adaptive antenna* is used for a phased array when the gain and the phase of the signals induced in the various elements are weighted before combining to adjust the gain of the array in a dynamic fashion along a particular look direction while placing nulls along the undesired directions. A block diagram of a typical adaptive antenna system is shown in Figure 3.1.

The propagation models used for an adaptive antenna are different from those for a single antenna. Details of a phased array antenna and joint estimation of channel parameters can be obtained in [6–8].

## 8.3 MULTIPATH PROPAGATION

In a typical mobile radio application, the base station is fixed in position while the mobile unit is moving, usually subject to such a condition that the propagation between them is largely through scattering, either by reflection or diffraction from buildings and terrain or objects within buildings, because of obstruction of the line-of-sight (LOS) path. Radio waves therefore arrive at the mobile receiver from different directions with different amplitude, phase, and time delays, resulting in a phenomenon known as *multipath propagation.* The radio channel is then obtained as the sum of contributions from all the paths.

If the input signal is a unit impulse, $\delta(\tau)$, the output will be the channel impulse response that can be written as [9]

$$h(t) = \sum_{n=1}^{N} A_n \, \delta(t - \tau_n) \exp(-j\varphi_n) \tag{8.8}$$

It can thus be characterized by $N$ time-delayed impulses, each represented by an attenuation and phase-shifted version of the original transmitted impulse. Here, $A_n$, $\tau_n$, and $\varphi_n$ are the attenuation, delay in time of arrival, and phase corresponding to path $n$, respectively. This model is only valid for a very narrowband signal. For a wideband signal the phase term has to be appropriately dealt with.

Although multipath interference seriously degrades the performance of communication systems, little can be done to eliminate it. However, if we characterize the multipath medium well and have sound knowledge of the propagation mechanisms and their influence on the system, the best design for the system can be selected to achieve good propagation performance and hence to achieve better quality of service.

### 8.3.1 Three Basic Propagation Mechanisms

Reflection, diffraction, and scattering are the three basic propagation mechanisms [10], that affect propagation in mobile communication systems. They are briefly explained below.

*8.3.1.1* ***Reflection.*** Reflection occurs when a propagating electromagnetic wave impinges upon an object that has very large dimensions compared to those of the wavelength of the propagating wave. Reflection occurs from the surface of the ground, walls, and furniture. When reflection occurs, the wave may also be partially refracted. The coefficient of reflection and refraction is a function of the material properties of the medium, and generally depends on the wave polarization, angle of incidence, and the frequency of the propagating wave.

*8.3.1.2* ***Diffraction.*** Diffraction occurs when the radio path between a transmitter and receiver is obstructed by a surface that has sharp edges. The waves produced by the obstructing surface are present throughout the space and even behind the obstacle, giving rise to bending of waves around the obstacle, even when a line-of-sight (LOS) path does not exist between the transmitter and receiver. At high frequencies, diffraction, like reflection, depends on the geometry of the object as well as the amplitude, phase, and polarization of the incident wave at the point of diffraction.

*8.3.1.3 Scattering.* Scattering occurs when the medium through which the wave propagates consists of objects with dimensions that are small compared to the wavelength, and where the number of obstacles per unit volume is large. Scattered waves are produced by rough surfaces, small objects, or by other irregularities in the channel. In practice, foliage, street signs, lampposts and stairs within buildings can induce scattering in mobile communication systems. Sound knowledge of the physical details of the objects can be used to accurately predict scattered signal strength.

In most cases, the scattering can be neglected [11] and the complex received field from the various incident paths is given by [12]

$$\vec{E}_{\text{receive}} = \sum_i \vec{E}_i \tag{8.9}$$

where

$$E_i = E_0 \wp_{ti} \wp_{ri} L_i(d) \prod_j \Gamma(\phi_{ji}) \prod_p T(\phi_{pi})\, e^{-jkd} \tag{8.10}$$

and

| | |
|---|---|
| $E_0$ | amplitude of the reference incident field (V/m) |
| $\wp_{ti}$ and $\wp_{ri}$ | transmitting and receiving antenna field radiation patterns along the direction of interest for the $i$th multipath component |
| $L_i(d)$ | path loss characterization for the $i$th multipath component |
| $\Gamma(\phi_{ji})$ | reflection coefficient for the $j$th reflection of the $j$th multipath component; |
| $T(\phi_{pi})$ | transmission coefficient for the $p$th transmission of the $i$th multipath component |
| $e^{-jkd}$ | propagation phase factor due to the path length $d$($k = 2\pi/\lambda$ with $\lambda$ representing the wavelength) |
| $d$ | path length (meters) |
| $E_i$ | field strength of the $i$th multipath component |

For diffraction, the product of the complex reflection and transmission coefficients is replaced by the complex diffraction coefficient.

### 8.3.2 Propagation in Outdoor and Indoor Environments

With the growth in the capacity of mobile communications, the size of a cell is becoming smaller and smaller from macrocell to microcell and then to picocell. The service environments include both outdoor and indoor areas.

When propagation is considered in an outdoor environment, one is interested primarily in three types of areas: urban, suburban, and rural. The terrain profile of a particular area also needs to be taken into account. The terrain profile may vary from a simple curved earth to a highly mountainous region. The presence of

trees, buildings, moving cars, and other obstacles must also be considered. Direct path, reflections from the ground and buildings, and diffractions from the corners, and roofs of buildings are the main contributors to the total field generated at a receiver due to radio-wave propagation.

There is also a great deal of interest in characterizing radio propagation inside buildings with the advent of personal communication systems (PCSs). The indoor radio channel differs from the traditional outdoor mobile radio channel in two aspects: the distance covered is much smaller, and the variability of the environment is much greater for a much smaller range of transmitter and receiver separation distance [10]. Propagation into and inside buildings has, to some extent, a more complex multipath structure than for an outdoor propagation environment. This is mainly because of the nature of the structures used for the buildings, the layout of rooms, and most important, the type of construction materials used. Table 8.1 represents the categories of buildings where propagation measurements have been made [13].

**TABLE 8.1**
Classification of buildings

| Category | Description |
|---|---|
| 1 | Residential houses in suburban areas |
| 2 | Residential houses in urban areas |
| 3 | Office buildings in suburban areas |
| 4 | Office buildings in urban areas |
| 5 | Factory buildings with heavy machinery |
| 6 | Other factory buildings, sports halls, exhibition centers |
| 7 | Open environment (e.g., railway stations, airports, etc.) |
| 8 | Underground (e.g., subways, underground streets, etc.) |

### 8.3.3 Summary of Propagation Models

In mobile communications, signals from the mobile arrive at a base station with multipaths, each with its own angle of arrival (AOA), path delay, and attenuation. When the communication system uses an adaptive processing methodology, it is also important to estimate joint angle and delay for various signals.

There are two main models for characterizing path loss, which are empirical (or statistical) models and site-specific (or deterministic) models. The former is based on the statistical characterization of the received signal. They are easier to implement, require less computational effort, and are less sensitive to the environment geometry. The latter has a certain physical basis and requires a vast amount of data regarding geometry, terrain profile, locations of building and furniture in buildings, and so on. These deterministic models require more computations and are more accurate.

Most models regarding fading apply stochastic processes to describe the distribution of the received signal. It is useful to use these models to simulate propagation channels and estimate the performance of the system in a homogeneous environment. Models of time delay spread both for outdoor and indoor environments are generally derived from a lot of measurements. In [142] some of the propagation models have been discussed and here we have included additional new models.

## 8.4 EMPIRICAL OR STATISTICAL MODELS FOR PATH LOSS

### 8.4.1 Outdoor Case

A number of empirical or statistical models are suitable for both macrocell and microcell scenarios for outdoor environment. Some of them are described below.

*8.4.1.1 Okumura et al. Model.* This is one of the most widely used models for propagation in urban areas [14]. The model can be expressed as

$$L_{50}(\text{dB}) = L_F + A_{mu}(f, d) - G(h_{te}) - G(h_{re}) - G_{\text{AREA}} \tag{8.11}$$

where $L_{50}$ is the median value of the propagation path loss, $L_F$ is the free-space propagation loss, $A_{mu}$ is the median attenuation in the medium relative to free space at frequency $f$, and $d$ corresponds to the distance between the base and the mobile, $G(h_{te})$ and $G(h_{re})$ are the gain factors for the base station antenna and mobile antenna, respectively, $h_{te}$ and $h_{re}$ are the effective height of the base station and the mobile antennas (in meters), respectively, and $G_{\text{AREA}}$ is the gain generated by the environment in which the system is operating. Both $A_{mu}(f,d)$ and $G_{\text{AREA}}$ can be found from empirical curves. Okumura et al.'s model is considered to be among the simplest and best in terms of accuracy in predicting path loss for early cellular systems. It is very practical and has become a standard for system planning in Japan. The major disadvantage of this model is its slow response to rapid changes in terrain profile.

*8.4.1.2 Hata Model.* It is an empirical formulation [15] of the graphical path loss data provided by Okumura's model. The formula for the median path loss in urban areas is given by

$$\begin{aligned} L_{50}(\text{urban})(\text{dB}) &= 69.55 + 26.16 \log f_c - 13.82 \log h_{te} \\ &\quad - a(h_{re}) + (44.9 - 6.55 \log h_{te}) \log d \end{aligned} \tag{8.12}$$

where $f_c$ is the frequency and varies from 150 to 1500 MHz, $h_{te}$ and $h_{re}$ are the effective height of the base station and the mobile antennas (in meters), respectively, $d$ is the distance from the base station to the mobile antenna, and $a(h_{re})$ is the correction factor for the effective antenna height of the mobile which is a function of the size of the area of coverage. For small to medium-sized cities, the mobile antenna correction factor is given by

$$a(h_{re}) = (1.1 \log f_c - 0.7)h_{re} - (1.56 \log f_c - 0.8) \text{ dB} \tag{8.13}$$

For a large city, it is given by

$$a(h_{re}) = 8.29(\log 1.54h_{re})^2 - 1.1 \text{ dB} \quad \text{for} \quad f_c \leq 300 \text{MHz} \tag{8.14a}$$

$$a(h_{re}) = 3.2(\log 11.75h_{re})^2 - 4.97 \text{ dB} \quad \text{for} \quad f_c \geq 300 \text{MHz} \tag{8.14b}$$

To obtain the path loss in a suburban area, the standard Hata formula is modified as

$$L_{50}(\text{dB}) = L_{50}(\text{urban}) - 2[\log(f_c/28)]^2 - 5.4 \tag{8.15}$$

The path loss in open rural areas is expressed through

$$L_{50}(\text{dB}) = L_{50}(\text{urban}) - 4.78(\log f_c)^2 - 18.33 \log f_c - 40.98 \tag{8.16}$$

This model is quite suitable for large cell mobile systems, but not for personal communications systems, which cover a circular area of approximately 1km in radius.

***8.4.1.3 COST-231–Walfisch–Ikegami Model.*** This utilizes the theoretical Walfisch–Bertoni model [16], and is composed of three terms [17]:

$$L_b = \begin{cases} L_0 + L_{rts} + L_{msd} & \text{for} \quad L_{rts} + L_{msd} > 0 \\ L_0 & \text{for} \quad L_{rts} + L_{msd} \leq 0 \end{cases} \tag{8.17}$$

where $L_0$ represents the free-space loss, $L_{rts}$ is the rooftop-to-street diffraction and scatter loss, and $L_{msd}$ is the multiscreen diffraction loss. The free-space loss is given by

$$L_0 = 32.4 + 20 \log d + 20 \log f \tag{8.18}$$

where $d$ is the radio-path length (in km), $f$ is the radio frequency (in MHz), and

$$L_{rts} = -16.9 - 10 \log w + 10 \log f + 20 \log \Delta h_{\text{Mobile}} + L_{ori} \tag{8.19}$$

Here $w$ is the street width (in m) and

$$\Delta h_{\text{Mobile}} = h_{\text{Roof}} - h_{\text{Mobile}} \tag{8.20}$$

is the difference between the height of the building on which the base station antenna is located, $h_{\text{Roof}}$, and the height of the mobile antenna, $h_{\text{Mobile}}$. $L_{ori}$ is given by

$$L_{ori} = \begin{cases} -10 + 0.354\phi & 0^\circ \le \phi < 35^\circ \\ 2.5 + 0.075\,(\phi - 35) & \text{for} \quad 35^\circ \le \phi < 55^\circ \\ 4.0 - 0.114\,(\phi - 55) & 55^\circ \le \phi \le 90^\circ \end{cases} \tag{8.21}$$

where $\phi$ is the angle of incidence relative to the direction of street. $L_{msd}$ is given by

$$L_{msd} = L_{bsh} + k_a + k_d \log d + k_f \log f - 9 \log b \tag{8.22}$$

where $b$ is the distance between the buildings along the signal path and $L_{bsh}$ and $k_a$ represent the increase of path loss due to a reduced base station antenna height. Using the abbreviation

$$\Delta h_{\text{Base}} = h_{\text{Base}} - h_{\text{Roof}} \tag{8.23}$$

where $h_{\text{Base}}$ is the base station antenna height, we observe that $L_{bsh}$ and $k_a$ are given through

$$L_{bsh} = \begin{cases} -18 \log(1 + \Delta h_{\text{Base}}) & h_{\text{Base}} > h_{\text{Roof}} \\ 0 & h_{\text{Base}} \le h_{\text{Roof}} \end{cases} \tag{8.24}$$

$$k_a = \begin{cases} 54 & & & h_{\text{Base}} > h_{\text{Roof}} \\ 54 - 0.8\,\Delta h_{Base} & d \ge 0.5\,km & \text{and} & h_{\text{Base}} \le h_{\text{Roof}} \\ 54 - 1.6\,\Delta h_{Base} d & d < 0.5\,km & \text{and} & h_{\text{Base}} \le h_{\text{Roof}} \end{cases} \tag{8.25}$$

The terms $k_d$ and $k_f$ control the dependence of the multiscreen diffraction loss versus distance and the radio frequency of operation, respectively. They are given by

$$k_d = \begin{cases} 18 & h_{\text{Base}} > h_{\text{Roof}} \\ 18 - 15\,\dfrac{\Delta h_{\text{Base}}}{h_{\text{Roof}}} & h_{\text{Base}} \le h_{\text{Roof}} \end{cases} \tag{8.26a}$$

and

$$k_f = -4 + 0.7\left(\frac{f}{925} - 1\right) \tag{8.26b}$$

for medium-sized cities and suburban centers with moderate tree densities and

$$k_f = -4 + 1.5\left(\frac{f}{925} - 1\right) \tag{8.26c}$$

for metropolitan centers.

This model is being considered for use by International Telecommunication Union-Radiocommunication Sector (ITU-R) in the International Mobile Telecommunications-2000 (IMT-2000) standards activities. Some improved solutions for diffraction by multiple absorbing half-planes have also been developed [18, 19]. Other solutions based on the uniform theory of diffraction (UTD) are also available [20, 21]. The performance of the various methods in estimating the multiple diffraction loss term and the final diffraction loss term is given in [22]. Recently, a correction to the COST-231–Walfisch–Ikegami Model has been reported [23].

***8.4.1.4 Dual-Slope Model.*** This is based on a two-ray model [24, 25] which is used commonly when the transmitting antenna is several wavelengths or more above the horizontal ground plane and suitable for the line-of-sight (LOS) propagation regions. The propagation loss, $L(d)$, in that case is described by a dual-slope model. This can be represented as a function $d$, the distance between the base station and the receiver. It is given by [26]

$$L(d) = L_b + \begin{cases} 10n_1 \log d + P_1 & 1 < d < d_{brk} \\ 10(n_1 - n_2)\log d_{brk} + 10n_2 \log d + P_1 & d \ge d_{brk} \end{cases} \tag{8.27}$$

where $P_1 = \text{PL}(d_0)$ and is the path loss in dB at the reference point $d_0$ and $d_{brk}$ represents the breakpoint or the turning point distance. The "point" where this transition occurs is often called the *Fresnel breakpoint*. $L_b$ is a basic transmission loss parameter which depends on frequency, and antenna heights $n_1$ and $n_2$ represent the slopes of the best-fit line before and after the breakpoint. If the transmitter and receiver antenna heights are known, along with the distance between them, the path loss can be computed based on the two parameters $n_1$ and

$n_2$. It is very reasonable to let $n_1 = 2$ for the region prior to the Fresnel breakpoint. There is much more variability in the path loss and the exponent for the region beyond the Fresnel breakpoint, with values of $n_2$ ranging from 2 to 7.

*8.4.1.5 Other Models*. Other models, including use of wideband measurements for different situations, have been discussed in recent times [27, 28, 141]. These models have been developed from measurements and use different parameters for different situations.

### 8.4.2 Indoor Case

Indoor radio propagation is not influenced by terrain profile as is outdoor propagation, but it can be affected by the layout in a building, especially if there exists various building materials. Owing to reflection, refraction, and diffraction of the radio wave by objects such as walls, windows, and doors inside a building, the transmitted signal often reaches the receiver through more than one path.

Distance/power model is the main propagation model for path loss. As shown in equation (8.3), many researchers estimate the rate of decay of a transmitter signal through this relation [29–34]. In an enclosed environment, the value of $\gamma$ in equation (8.3) may be 1.5 to 1.8 when the transmitter and receiver are placed in the same hallway and are in sight of each other. When the receiver is located within a room off the hallway, $\gamma$ ranges from 3 to 4 [30–33]. $\gamma$ also varies with frequency [33] and is dependent on building materials used in a particular environment [34]. References [5] and [32] provide reviews on early works of these models. Table 8.2 [29] shows the parameters of (8.3) determined by measurement for different buildings [35–40].

**TABLE 8.2**
Path loss measured in different buildings

| Building | $\gamma$ | PL (dB) | Frequency (MHz) | Ref. |
|---|---|---|---|---|
| Grocery store | 1.8 | 5.2 | 914 | [35] |
| Retail store | 2.2 | 8.7 | 914 | [35] |
| Open-plan factories | 2.2 | 7.9 | 1300 | [36] |
| | 1.4–3.3 | — | 910 | [37] |
| Open-plan factories B | 2.0 | 3.7 | 1300 | [38] |
| | 2.1 | 4.0 | 1300 | [38] |
| Open-plan factories C | 2.4 | 9.2 | 1300 | [38] |
| | 2.1 | 9.7 | 1300 | [38] |
| Suburban office building open plan | 2.4 | 9.6 | 915 | [39] |
| | 2.6 | 14.1 | 1900 | [39] |
| Suburban office building soft partition | 2.8 | 14.2 | 915 | [39] |
| | 3.8 | 12.7 | 1900 | [39] |
| | 3.0 | — | 850 | [40] |

In order to take into account the attenuation due to walls and floors, two additional terms are added to (8.3) to result in [35, 41]

$$\mathrm{PL}(d) = \mathrm{PL}(d_0) + 10n\log(d/d_0) + \sum_{q=1}^{Q} \mathrm{FAF}(q) + \sum_{p=1}^{P} \mathrm{WAF}(p) \qquad (8.28)$$

where FAF($q$) and WAF($p$) are the floor and wall attenuation factors, respectively. Table 8.3 lists the FAFs for two buildings [29, 30].

It is also observed that the propagation path loss as a function of the distance also has two distinct regions for indoor environments [42], as described in (8.28). When electromagnetic radiation is incident on a wall or a floor in an oblique fashion, less power will be transmitted through the wall than would occur at normal incidence. Reference [41] modifies the term of WAF($p$) as WAF($p$)/cos $\phi_p$ and FAF($q$) as WAF($q$)/cos $\phi_q$, where WAF($p$) and FAF($q$) are the values of the attenuation factors at normal incidence. $\phi_p$ and $\phi_q$ are the angles of incidence of the signal on the walls and floors, respectively. A diffraction term has also been added to the formula in [41]. When the base station is out of the building, the path loss in the building has been given in [43].

These empirical or statistical models described in this section are simple to implement and are used widely when the accuracy of the data is not a critical requirement.

**TABLE 8.3**
Average Attenuation Factor (FAF)

| Location | FAF (dB) | PL (dB) |
|---|---|---|
| Office building 1 | | |
| Through 1 floor | 12.9 | 7.0 |
| Through 2 floors | 18.7 | 2.8 |
| Through 3 floors | 24.4 | 1.7 |
| Through 4 floors | 27.0 | 1.5 |
| Office building 2 | | |
| Through 1 floor | 16.2 | 2.9 |
| Through 2 floors | 27.5 | 5.4 |
| Through 3 floors | 31.6 | 7.2 |

## 8.5 SITE-SPECIFIC MODELS FOR PATH LOSS

*Site-specific propagation models*, also called *deterministic models*, are based on the theory of electromagnetic-wave propagation. Unlike statistical models, site-specific propagation models do not rely on extensive measurements but on

greater detail of the environment and provides an accurate prediction of the signal propagation.

In theory, propagation characteristics of electromagnetic waves could exactly be computed by solving Maxwell's equations. Unfortunately, this approach requires very complex mathematical operations and requires considerable computing power. In [44], this method has been applied to simplified environments.

### 8.5.1 Ray-Tracing Technique

Ray tracing is a technique based on geometrical optics (GO), which can easily be applied as an approximate method for estimating levels of high-frequency electromagnetic fields. GO assumes that energy can be considered to be radiating through infinitesimally small tubes, often called *rays*. These rays are normal to the surface of equal signal power, and lie along the direction of propagation and travel in straight lines, provided that the relative refractive index of the medium is constant. Therefore, signal propagation can be modeled via ray propagations. By using the concept of ray tracing, rays can be launched from a transmitter location and the interaction of the rays can be described using the well-known theory of refraction and reflection and interactions with the neighboring environment. In GO, only direct, reflected, and refracted rays are considered, and consequently, abrupt transition areas may occur, corresponding to the boundaries of the regions where these rays exist. The geometrical theory of diffraction (GTD) and its uniform extension, the uniform GTD (UTD) [45], complement the GO theory by introducing a new type of rays, known as *diffracted rays*. The purpose of these rays is to remove the field discontinuities and to introduce proper field corrections, especially in the zero field regions predicted by GO.

The Fermat principle and the principle of local field are two basic concepts used extensively by ray models. The Fermat principle states that a ray follows the shortest path from a source point to a field point, while the principle of the local field states that when hitting a surface, the high-frequency rays produce reflection, refraction, and diffraction. This depends only on the electrical and geometrical properties of the scatterer in the immediate neighborhood of the point of interaction.

The ray-tracing method is widely used in propagation model and system design [12, 42, 46–72, 145]. It is most accurate when the point of observation is many wavelengths away from the nearest scatterer. All scatterers are assumed to be large, compared to a wavelength. Two types of ray-tracing methods, namely the image method [12, 48, 55, 58] and the brute-force ray-tracing method, are generally used. They are now explained.

***8.5.1.1 Image Method.*** This method generates the images of a source at all planes. These images then serve as secondary sources for subsequent points of reflections. If there are $N$ reflecting planes, there are $N$ first-order (i.e., one-

reflection) images of a source, $N(N-1)$ two-reflection images, $N(N-1)(N-1)$ three-reflection images, and so on [48]. To determine whether an image of the source is visible at the destination is to trace the intersection of the reflected ray at all necessary planes of interest. Thus, the energy reaches the destination through multiple reflections and contributes to the received power. Once a ray has been traced through all its reflections to the source, the attenuations associated with all the reflection terms are calculated.

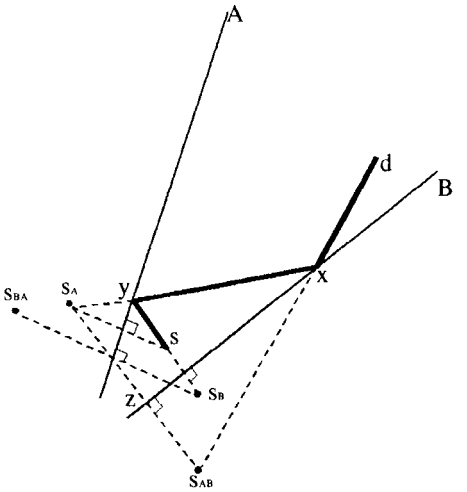


**Figure 8.3.** Images due to a source placed between two mirrors, A and B.

Image method is efficient but can handle simple environments only. Many environments with which we are concerned in our daily life are complicated, and the conventional image method is not adequate. Figure 8.3 shows a source and its images corresponding to two reflections [48]. The concept of a lit region has been introduced in [58] and is illustrated in Figure 8.4. Behind the plate representing a building where the image is formed, the region is termed the *unlit domain*. For the 2D case, only reflections from walls and diffraction from corners in buildings are taken into account. Ground reflection and rays over rooftops are neglected [58]. In [53–55] a modified shooting-and-bouncing-ray technique, combined with the image method, has been used to deal with the radio wave propagation in furnished rooms. The effects of diffraction have also been considered. A threshold must be set with respect to the number and order of reflection and diffraction rays that can be considered.

*8.5.1.2* ***Brute-Force Ray-Tracing Method.*** This method considers a bundle of transmitted rays that may or may not reach the receiver. The number of rays considered and the distance from the transmitter to the receiver location

determines the available spatial resolution and hence the accuracy of the model. This method requires more computing power than the image method.

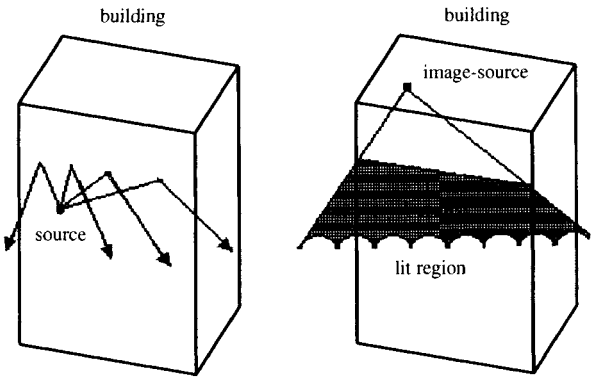


**Figure 8.4.** The reflection by a wall in a building is modeled by an image source placed behind it and a lit region in front of it.

A finite sample of the possible directions of the propagation from the transmitter is chosen. For each such direction, a ray is launched. If a ray hits a wall, a reflecting ray and refracting ray are generated. If a ray hits a wedge, a family of diffracting rays is generated. A reception sphere with the correct radius can describe a region that will receive exactly one ray. If the radius is too large, two rays could be received and the same specular ray may be counted twice. If the radius is too small, it is possible that none of the rays will reach the reception sphere and the specular ray will be excluded [42, 59]. Figure 8.5 shows the proper size of the reception sphere which may receive a ray. For each receiver location, the perpendicular distance $d$ from the receiver to the ray is computed together with the total (unfolded) ray path length $L$ from the source to the perpendicular projection point. If $d$ is greater than or equal to $(\phi L)/2$ for the 2D case or $(\phi L) / \sqrt{3}$ for the 3D case, the ray is treated as not having reached the receiver location. Here $\phi$ is the angle between two rays. Otherwise, the ray is considered to be contributing to the received signal. There is no reception sphere associated with use of the image method.

The key part of the ray-tracing method is the generation and description of the rays. There are two kinds of methods to obtain the rays at the source point. One is a 2D approach, the other is a 3D method.

- ***2D ray-tracing model*** [42]. In two dimensions, all the rays or ray tubes are treated as ray sectors, as shown in Figure 8.6. At the source, rays are launched along different directions with the same sector angle $\phi$ in a plane. How to choose the angle $\phi$ depends on the accuracy required and the computation time. If the

angle is small, it will provide high accuracy and will take much time to compute. For example, if the angle $\phi = 1°$, then there will be 360 rays to be traced.

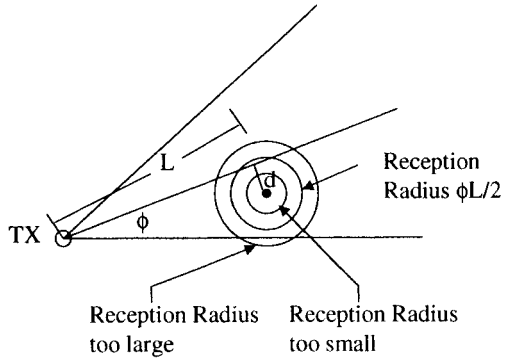


**Figure 8.5.** Reception sphere for a 2D ray tracing.

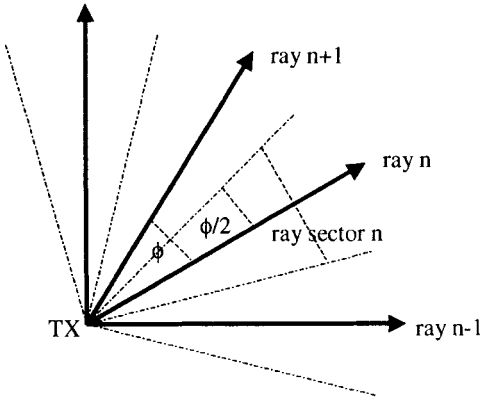


**Figure 8.6.** Rays generated from a source in two dimensions.

Each ray is launched from the source and can be traced through a binary tree. An intersection with a surface of an object is represented by a node in the tree. The incident ray is decomposed into an object-reflected ray and an object-penetrated ray. It is assumed that the reflected ray propagates along the specular direction (incidence angle equals the aspect angle) and the ray that penetrates the object keeps the original direction of the incident ray. Both rays then propagate to the next intersection. An intersection with a wedge is also represented by a node, and the diffraction point is processed as a source and a large number of rays must be launched. The decomposition process is repeated as a recursion

process. This procedure is continued until the rays are weaker than an assumed threshold, leaves a predefined propagation area, or is received. The strength of the field at the receiver is then calculated according to (8.9).

A 2D diffraction model has been introduced in [62, 64]. The various buildings are considered as vertical knife-edges, neglecting the over-rooftop diffraction and ground reflection. Because the buildings are much higher than the base station (BS) and mobile station (MS) antennas in an urban microcellular environment, the weak contribution from the signals from the over-rooftop rays can be neglected. No rays due to a single ground reflection from the transmitter to the receiver exist in the shadow regions. For ranges less than 1 km from a transmitter (primary source), the received power may have a range $R$ dependence according to the power law of $1/R^2$. However, for LOS regions, the ground reflections appear to be less important.

As reported in [64], the 2D ray-tracing algorithm is quite accurate when the transmitting and receiving antenna heights are much below the rooftops of the surrounding buildings. This propagation model between a transmitter and receiver located close to the ground is usually called the *canyon model.*

When using a 2D model, the inputs are: (1) 2D geometry described by means of vectors specifying the location of the building walls; (2) estimated electrical characteristics of the building walls (permittivity and conductivity or the scalar reflection coefficient); (3) base-station location; (4) antenna pattern, and (5) frequency of operation.

- ***3D ray-tracing model*** [12, 64–72]. The transmitter and receiver are modeled as point sources when using this ray-tracing technique. In order to determine all possible rays that may leave the transmitter and arrive at the receiver in three dimensions, it is necessary to consider all possible angles of departure and arrival at the transmitter and receiver. Rays are launched from the transmitter at an elevation angle $\theta$ and with an azimuth angle $\varphi$ as defined in the usual coordinate system. Antenna patterns are incorporated to include the effects of antenna beamwidth in both azimuth and elevation.

To maintain all the ray manipulation routines as general, it is desirable that each ray tube occupies the same solid angle $d\Omega$, and each wavefront has an identical shape and size at a distance $r$ from the transmitter. Additionally, these wavefronts must be such that they can be subdivided so that an increased ray resolution can be handled easily. For example, let $r = 1$ and the total wavefront be the surface of a unit sphere. The problem then becomes one of subdividing the sphere surface into areas of equal "patches" so that all are of the same size and shape and collectively covers the surface of interest without gaps. Hexagonal [12] and triangular [53, 54] ray wavefronts have also been used.

The procedure of ray tracing in 3D is similar to a 2D model, but more computational time is needed.

Some sectors of the walls in a corridor thus can be made of different materials, for example, wood, metal, concrete, or even glass, which may have different reflectivity for the incident wave. Neglecting the differences between the reflectivities of the various materials will degrade, predicting the accuracy of

the propagation model. Therefore, in [12] it is proposed to have the concept of an *effective building material* to represent the physical and complicated constitutive materials used in the walls of a building. However, permittivity of this effective material is not easy to determine since it depends on the experimental data as well as on the propagation model. To simplify this problem, patches of different dielectric constants and physical sizes have been introduced in [65]. It is noted that the size and dielectric constant of each patch are chosen according to their physical dimensions and the material it is made of.

The key to a propagation model based on ray tracing is to find a computationally fast way to determine the dominant ray paths so as to provide accurate pathloss predictions. It is well known that for outdoor propagation prediction, in addition to specular reflections, diffraction from edges must be accounted for, especially in non-LOS regions. Unfortunately, diffractions are very time consuming to model since a single incident ray encountering an edge will generate an entire family of new rays. The generation of a large number of diffracted rays limits the number of diffractions that can be considered. For any given path we choose at most two, unless an approximation can be made to find the important contributing rays. In order to find the contributing rays in an urban environment where the building walls are nearly always vertical planar polygons, a vertical-plane-launch (VPL) method has been developed [66]. The VPL approach accounts for specular reflections from vertical surfaces and diffraction at the vertical edges and approximates diffraction along horizontal edges by restricting the diffracted rays to lie in the plane of incidence or in the plane of reflection. The VPL approach can treat many multiple forward diffractions at horizontal edges. It can also be used for rooftop antennas and areas where there exist buildings of different heights.

To improve the efficiency of ray-tracing models, many researchers have developed a large number of methods [68, 72]. In [68], a hybrid technique has been presented where the object database is held in two dimensions, but a ray-tracing engine operates in three dimensions. The 3D rays are produced by combining the results of two 2D ray tracers, one on a horizontal and the other on a vertical plane. Moreover, by significantly enhancing the concept of illumination zones the performance of the algorithm can be dramatically improved.

Comparison of 2D and 3D models has been made in [64].

### 8.5.2 Finite-Difference Time Domain Models

Based on geometrical optics (GO) and usually supplemented by UTD, a ray-tracing algorithm provides a relatively simple solution to radio propagation. However, it is well known that GO provides good results for electrically large objects and UTD is rigorous only for perfectly conducting wedges. For complex lossy structures with finite dimensions, ray-tracing fails to predict correctly the scattered fields. In a complicated communication environment, transmitting and receiving antennas are often inevitably installed close to a structure with complex

material properties, for which no asymptotic solutions are available. Such problems can be solved by numerical solution of Maxwell's equations. In particular, the finite-difference time domain (FDTD) method is an alternative. The advantages of the FDTD method are its accuracy and that it simultaneously provides a complete solution for all the points in the map, which can give signal coverage information throughout a given area.

In a simple outdoor environment, a two-dimensional FDTD is generally applied [73]. A simple approach for introducing the correct spherical wave spreading has been developed. A comparison with the FDTD predictions could be used to evaluate and refine the GTD-based methods.

A reduced formulation for the standard FDTD technique [74], requiring four scalar field components instead of the usual six, is used to predict channel statistics inside a residential building. Measurements have also been conducted and results compared with simulated data. In order to introduce arbitrary-shaped antennas into the simulations, a two-and-a-half dimension (2.5D) or a multimode FDTD method has been established for indoor radio propagation calculations [75].

A hybrid technique [76] based on combining a ray-tracing method with FDTD method for more accurate modeling of radio wave propagation has also been suggested. The basic idea is to use ray tracing to analyze wide areas and FDTD to study areas close to structure with complex material properties, where ray-based solutions are not sufficiently accurate.

As a numerical method, FDTD requires large amounts of computer memory to keep track of the solution at all locations, and extensive calculations to update the solution at successive instants of time. Application of an accurate numerical analysis method to model an entire area is neither practical because of the computational resource required, nor is it necessary for open areas without many objects.

### 8.5.3 Moment Method Models

Ray-tracing models can be used with sufficient precision to predict radio coverage for large buildings having a large number of walls between the transmitter and the receiver, while the moment method (MM) model is better when higher precision is required and the size of the buildings is smaller. A combination of these two models is also possible using the advantages of each. Where a lot of small but dominant obstacles are present or paths that cannot be taken into account by a ray-tracing model, the MM model can be used [77, 78].

The solutions determined by MM are numerically exact as long as the spatial segmentation used for the objects is small enough. Due to the limitations of the computer memory and CPU time, the MM is generally used to analyze objects which are tens of wavelengths in size. However, by choosing structures with dimensions around a few wavelengths, the MM can be used to check and verify the ray-tracing program. A 2D problem, which includes stair-shaped walls above

a lossy ground, was simulated by using both the MM and ray-tracing methods [77].

The transmission of an UHF wave through a window in a wall is critical when integrating systems that include both indoor and outdoor areas. A novel simulation approach based on the moment method is presented in [79]. In the simulations, the walls have been modeled as two long dielectric slabs, long enough so that any diffraction or reflection at the outer edges would not influence the results. No distinction has been made between the concrete and brick parts. The glass plates have also been assumed to be homogeneous and the aluminum frame was modeled as a perfectly conducting material. The resulting simulations are then compared to a set of measurements, where good agreement has been achieved.

A hybrid approach combining the ray-tracing method and the periodic moment method (PMM) for material objects has been developed to study the indoor wave propagation, penetrations, and scattering due to periodic structures in buildings [80]. The PMM is applied to evaluate the specular and grating transmission and reflection coefficients of the periodic structures. Those data are then used in a ray-tracing program to find the specular and grating rays for each ray tube illuminating one of the periodic structures. Those excited ray tubes are continuously traced to determine their contributions to the receiving antennas.

### 8.5.4 Artificial Neural Network Models

The main problem with the statistical models is usually the accuracy, while the site-specific models lack computational efficiency. Artificial neural networks (ANNs) have shown very good performance in solving problems with mild nonlinearity on a set of noisy data. This case corresponds to a problem at a field-level prediction, as the data obtained from measurements is always noisy. Another key feature of the neural networks is the intrinsic parallelism, allowing for fast evaluation of the solutions.

The ANN model [81], which has the form of a multilayer perception, is generally used with 12 inputs and one output. It has been developed to predict the propagation in an indoor environment. In this case, a 2D floor plan is used for a database with a resolution of $10 \times 10$ cm. All particular locations are classified into 11 distinct categories, such as wall, corridor, outdoor area, laboratory, and so on. One input of the network represents the normalized distance from the transmitter to the receiver. In addition, there is an input for each defined environment category. Other inputs represent either a normalized number of occurrences (doors and windows) or an appropriate percentage (wall, corridor, and so on) of that category along the straight line drawn from the transmitter to the receiver. The process of learning may last for a couple of hours, but the process for field-level prediction is fast. The accuracy of a prediction model significantly depends on the accuracy of the environment databases.

In [82], theoretical investigations into the suitability of a neural network simulator for the prediction of field strength based on topographical and

morphographical data are presented. Effective input and output data processing is developed using a deterministic and heuristic formula for the training of a neural network simulator. The network used is similar to that described in [81]. The inputs are frequency, heights of the antenna for a base and mobile stations, respectively, and the distance between them. The output is the field strength.

Although the multilayer neural network [82] is a useful method for approximating the propagation loss, however, it suffers from drawbacks of slow convergence and unpredictable solutions during learning. To overcome this difficulty, radial basis function (RBF) neural networks that have a "linear in the parameters" representation are proposed to enhance the real-time learning capability and achieve a rapid convergence [83]. The RBF neural network is a two-layer localized receptive field network whose output nodes form a combination of radial activation functions computed by the hidden layer nodes. Appropriate centers and connection weights in the RBF network lead to a network that is capable of forming the best approximation to any continuous nonlinear mapping up to an arbitrary resolution. Such an approximation introduces best nonlinear approximation capability into the prediction model in order to accurately estimate the propagation loss over an arbitrary environment based on adaptive learning from measurement data. Okumura's data are often included to demonstrate the effectiveness of the RBF neural network approach.

### 8.5.5 Other Models

Recently, many new methods have been introduced to predict propagation for mobile communications. Some of them are described here.

*8.5.5.1 **Parabolic Equation Model.*** This is applied to the modeling of radio-wave propagation in an urban environment. As a parabolic version of Maxwell's equations it allows full treatment [84, 138, 139] of 3D electromagnetic scattering which is not possible with scalar versions of the algorithm. It is particularly useful for accurate modeling of scattering by a single building or a group of buildings at microwave frequencies. Examples include scattering by a building with a hemispherical roof and scattering by a group of buildings with sloping roofs.

*8.5.5.2 **Fast Far-Field Approximation Model.*** This is substantially faster than conventional integral-equation (IE)-based techniques. The technique is improved by incorporating the Green's function perturbation method. The method has been applied to gently undulating terrains and compared to published experimental results in the 900-MHz band. It has also been successfully applied to more hilly terrain and to surfaces with added buildings [85]. An improved version of the "shifting function" has been introduced, which can improve the performance of the technique for more challenging problems such as scattering from a wedge.

The issues of profile truncation and small-scale roughness effects have been addressed, and numerical results presented show excellent agreement with published measured data.

*8.5.5.3 Waveguide Model.* In large metropolitan areas which have tall buildings, the transmitting and receiving antennas are both located below the rooftops and the city streets act as a type of waveguiding structure for the propagating signal [86, 87, 140]. In this case, there is a need to develop efficient algorithms for the computation and mapping of the field distribution in such structures. Theoretical analysis of propagation in a city street modeled as a 3D multislit waveguide is proposed. Assuming that the screens and slits are distributed by a Poisson law, the statistical propagation characteristics in such a waveguide are expressed in terms of multiple ray fields approaching the observer. Algorithms for path loss prediction have been presented and compared with experimental data in the two references cited above.

*8.5.5.4 Boltzmann Model.* This was initially developed for simulated fluid flows. It describes a physical system in terms of the motion of fictitious microscopic particles on a lattice [88, 143]. This technique can take complicated boundary conditions into account. Two-dimensional simulations have been performed starting from a city map and a renormalization scheme has been proposed. The method, which is simple and easy to implement, provides good path loss predictions compared with on-site measurements.

## 8.6 SUMMARY OF MODELS FOR PATH LOSS

A summary of the various propagation models dealing with path loss has been reviewed. A brief comparison of some of the main models is presented in Table 8.4. Propagation models dealing with path loss for mobile communication have been emphasized using two very different approaches. First, a simple empirical or statistical model of the path loss has been considered where some of the parameters used are determined empirically from measurements. The second approach used is site-specific methods. Ray tracing is the main method. Some other numerical methods used in electromagnetic fields computation have also been applied.

Each of these two kinds of approaches makes a very different trade-off of accuracy versus complexity. The empirical (statistical) models are extremely simple (no environmental information is used other than of a very type in the choice of the parameters), but the predictions are not very accurate. On the other hand, site-specific models are considerably more accurate than the empirical models, but require a great deal of specific information about the area of interest (the locations of all the objects at a minimum and possibly the locations of large objects).

**TABLE 8.4**
Comparison of models for path loss

| Model Name | Suitable Environment | Complexity | Experimental Data | Details of Environment Request | Accuracy | Time | Other |
|---|---|---|---|---|---|---|---|
| Okumura model | Macrocell | Simple | Based on experiments | No | Good | Little | Graphical path loss data |
| Hata model | Macrocell (early cellular) | Simple | No | No | Good | Little | |
| Cost-231 | Microcell (outdoor) | Simple | No | No | Good | Little | |
| Dual-slope | Microcell and picocell (LOS region) | Simple | No | No | Good | Little | |
| Ray-tracing | Outdoor and indoor | Complex | No | Yes | Very good | Very much | |
| FDTD | Indoor (small) | Complex | No | Every detail | Best | Very much | Often combined with ray-tracing |
| MOM | Indoor (small) | Complex | No | Every detail | Best | Very much | |
| ANN | Outdoor and indoor | Complex | Yes | Detail | Very good | Little | Take time to learn from experimental data |

## 8.7 EFFICIENT COMPUTATIONAL METHODS FOR PROPAGATION PREDICTION FOR INDOOR WIRELESS COMMUNICATION

This section presents two different deterministic methods for efficient characterization of an indoor channel. First an improved version of a ray-tracing method is presented. Next the finite-difference-time-domain (FDTD) method is used to calculate the effects of walls in an indoor wave propagation environment.

### 8.7.1 Efficient Ray-Tracing Methods

The application of several ray-tracing techniques in combination with the uniform theory of diffraction is an efficient method for prediction of propagation in the UHF (communication) band in an indoor environment. This is discussed in detail [136] as we improve the computational efficiency of the two-dimensional (2D) ray-tracing method by reorganizing the objects in an indoor environment into irregular cells. In addition, by making use of the 2D ray-tracing results, a new three-dimensional (3D) propagation prediction model is developed, which can save 99% of the computation time of traditional 3D model. This new hybrid model is more accurate than 2D models and more efficient than traditional 3D models in computing the path loss to any point in the building. In this model,

reflection and refraction by layered materials and diffraction from the corners of the wall are considered.

As shown in Figure 8.7 there are four main types of rays from the transmitter to the receiver. There are two types of ray-tracing methods, one is called the *image method* [53, 54, 57] and the other is the *brute force ray-tracing method* [12, 42]. The image method is well suited to analysis of radio propagation associated with geometry of low complexity and with small number of reflections. The brute-force method launches a bundle of rays that may or may not reach the receiver. It requires numerous ray object intersection tests and extensive data arrays for ray tracing. In the brute-force method, both refraction and diffraction can be considered. In these two methods, both the 2D and 3D ray-tracing models are used widely. In the 2D model, only those rays in a plane are traced, so it needs less computation time. In the 3D model, all rays must be traced, so it needs much more computation time.

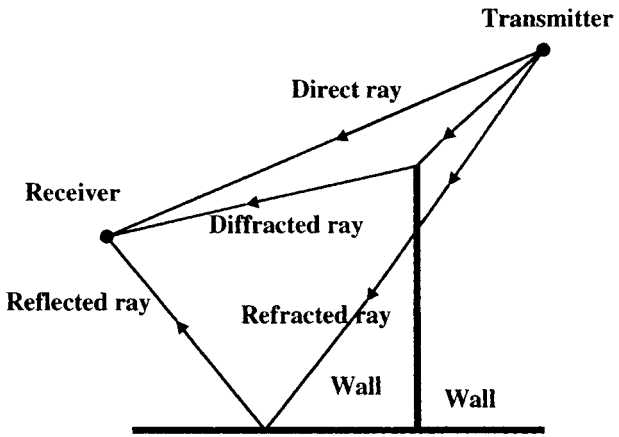


**Figure 8.7.** Four main types of rays in an indoor environment.

2D ray-tracing technique is widely used for indoor propagation prediction [58, 128, 129]. When the indoor environment is large and complex, it will take much CPU time to calculate the propagation characteristics. It is therefore important to improve the computational efficiency. In [128, 129], only those rays that have certain contribution to the receiver are traced. In [130], effective-propagation-area method and dominant-corner extraction method are used. However, by making use of the geometrical characteristics of an indoor environment and reorganizing the objects, a new 2D ray-tracing model termed an irregular cell model is presented. Almost 60% of the CPU time can be saved using this technique and without any loss in accuracy.

Based on that, we develop a new efficient 3D ray-tracing model that integrates several improved ray-tracing techniques. In this model, all objects are projected onto the floor. By using a 2D ray-tracing algorithm and a suitable selection of an elevation angle, all effective rays (which can reach the receiver) can be determined. Because fewer effective rays need to be traced, much computation time can be saved. In addition, the patched-wall technique and the ray-fixed coordinate system, respectively, are used in the analysis in order to improve the computation accuracy and to reduce the dimension (from three to two) for the dyadic characterization of reflection, refraction, and diffraction coefficients. The computation results are validated by measurements carried out in a building at Shanghai Jiao Tong University at 1.7 GHz.

***8.7.1.1 Rays in an Indoor Environment.*** As shown in Figure 8.7, the direct ray makes the main contribution to the received signal, if it exists. When the receiver is out of sight from the transmitter, reflected, refracted, and diffracted rays carry energy to the receiver. They are expanded as follows.

- ***Reflected and refracted rays.*** In an indoor environment, objects always have a certain thickness, as shown in Figure 8.8. In addition, they also introduce losses. Generally, when a ray in air illuminates an object, a reflected ray and a refracted ray are produced in the upper and lower areas of the space, respectively. The reflected ray can be considered as the rays coming from the mirror image of the object. The refracted ray in the lower area of the space is parallel to the incident ray, but it has a deviation $\Delta d$, as shown in Figure 8.8. The deviation is given by

$$\Delta d = d \sin(\phi_i - \phi_t) / \cos\phi_t \tag{8.29}$$

where $\phi_i$ and $\phi_t$ are the angles of incidence and refraction, respectively. In an indoor environment, the thickness of a typical wall is 20 to 30 cm, so the general distance between the refracted ray and the incident ray may be less than 20 cm. If the wall is thicker, the refracted ray may be too weak to be considered in the calculations. When using a ray-tracing technique, the ray is considered as a tube and it diffuses as it propagates. For example, assume the angle of the tube to be 1°; the radius of its wavefront will be 17.46 cm after it propagates a distance of 20 m. At most, it is reasonable to ignore the offset between the refracted ray, and the incident ray as has been done in most papers. In [131], an equivalent source is introduced to consider this offest. On modern interior walls which are construced from two layers of gypsumboard nailed onto the studs, the offset is also very small. Sometimes, there are multiple reflections within the wall, and the offset between the first reflected ray and other higher-order reflected rays can be treated in a fashion similar to that used for the refracted ray.

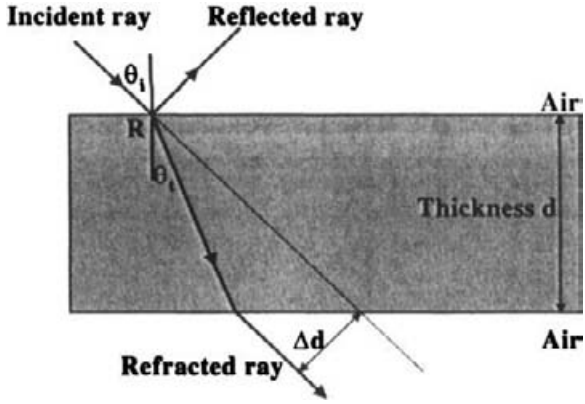


**Figure 8.8.** Typical reflected and refracted rays in an indoor environment.

The coefficients of reflection ($R$) and refraction ($T$) for layered lossy materials are given by (8.30) [132]. It is assumed that there are $n$ layers of homogeneous and nonmagnetic lossy materials. Layer 1 and layer $n$ are the air regions. One can therefore write

$$\begin{bmatrix} 1 \\ R^{\perp//} \end{bmatrix} = [U_{1n}] \begin{bmatrix} T^{\perp//} \\ 0 \end{bmatrix} \tag{8.30}$$

where $[U_{1n}] = [U_{12}][U_{23}] \cdots [U_{(n-1)n}]$ with

$$[U_{i(i+1)}] = \frac{1}{2}\left[1 + \frac{k_{(i+1)x}}{k_{ix}}\right] \begin{bmatrix} e^{jk_{(i+1)x}d_i} & R_{i(i+1)}e^{-jk_{(i+1)x}d_i} \\ R_{i(i+1)}e^{jk_{(i+1)x}d_i} & e^{-jk_{(i+1)x}d_i} \end{bmatrix}$$

$k_i$ = wavenumber of medium $i = \omega\sqrt{\varepsilon_i \mu_0}$

$k_{ix}^2 = k_i^2 - (k_1 \sin\theta)^2$, for $i = 1, 2, \ldots, n-1$

$d_i$ = thickness of layer $i$ with ($d_1 = d_n = 0$)

$\varepsilon_i$ = complex dielectric constant of layer $i$

$\phi$ = angle of incidence

$\omega$ = angular frequency of the incident ray

Superscripts $\perp$ and // represent the perpendicular polarization and parallel polarization, respectively. The values for the reflection coefficients for different polarizations are given by

$$R^{\perp}_{i(i+1)} = \frac{1 - \dfrac{k_{(i+1)x}}{k_{ix}}}{1 + \dfrac{k_{(i+1)x}}{k_{ix}}} \quad \text{for perpendicular polarization,}$$

and

$$R^{//}_{i(i+1)} = \frac{1 - \dfrac{\varepsilon_i k_{(i+1)x}}{\varepsilon_{i+1} k_{ix}}}{1 + \dfrac{\varepsilon_i k_{(i+1)x}}{\varepsilon_{i+1} k_{ix}}} \quad \text{for parallel polarization for } i = 1, 2, \ldots, n-1.$$

When a ray-fixed coordinate system is used, reflected field $\vec{E}_r(R)$ at a position $R$ is determined from the incident field $\vec{E}_i(R)$ at position $R$ by using the following equation:

$$\begin{bmatrix} E_r^{\perp} \\ E_r^{//} \end{bmatrix} = \begin{bmatrix} R^{\perp} & 0 \\ 0 & R^{//} \end{bmatrix} \begin{bmatrix} E_i^{\perp} \\ E_i^{//} \end{bmatrix} \tag{8.31}$$

We have a similar relation to obtain the refracted field at the position $R$, by substituting the reflection coefficients $R^{\perp}$ and $R^{//}$ with the respective transmission coefficients by $T^{\perp}$ and $T^{//}$, respectively, with $T^{\perp}$ and $T^{//}$ given by (8.30).

The magnitude of the reflection coefficients $|R|$ at 1.8 GHz for various materials is shown in Figure 8.9. Some of the materials described, for example, are wall (thickness $d = 20$ cm, $\varepsilon_r = 3.25$), a wooden door ($d = 4$ cm, $\varepsilon_r = 1.94$), and a glass window ($d = 0.4$ cm, $\varepsilon_r = 3.95$). From this figure it can be seen that the magnitude of the reflection coefficient for all the materials are close to 1 when the incident angle is close to 90°.

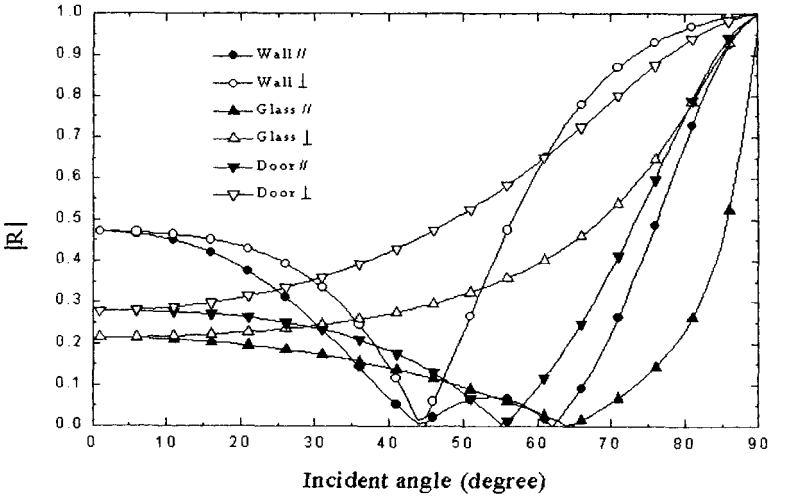


**Figure 8.9.** Magnitude of the reflection coefficients as a function of polarization for different materials.

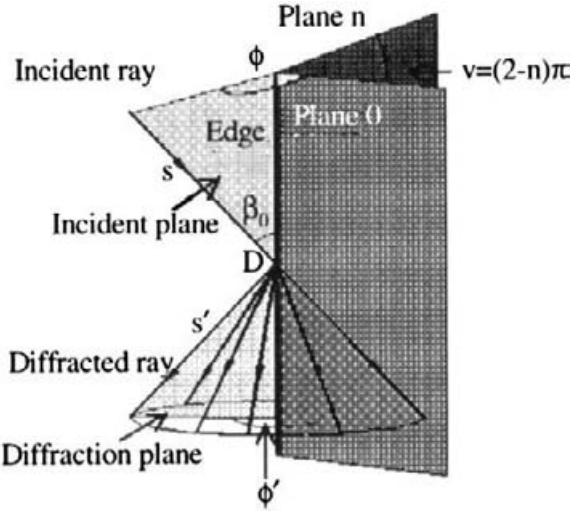


**Figure 8.10.** Diffraction due to a corner.

• ***Diffracted ray.*** The uniform theory of diffraction (UTD) is applied to calculate the diffracted field from the corners in an indoor environment. In Figure 8.10 a wedge with an angle $(2-n)\pi$ is used for illustration purposes. The field is

incident on it at an oblique angle. The coefficients of diffraction $D^{\perp//}$ are given by [54]

$$
\begin{aligned}
D^{\perp//} = \frac{-e^{-j\pi/4}}{2n\sqrt{2\pi k}\sin\beta_0}\Bigg\{ & \cot\frac{\pi+(\phi'-\phi)}{2n}F[kLa^{+}(\phi'-\phi)] \\
& + \cot\frac{\pi-(\phi'-\phi)}{2n}F[kLa^{-}(\phi'-\phi)] \\
& + R_0^{\perp//}\cot\frac{\pi-(\phi+\phi')}{2n}F[kLa^{-}(\phi+\phi')] \\
& + R_n^{\perp//}\cot\frac{\pi+(\phi+\phi')}{2n}F[kLa^{+}(\phi+\phi')]\Bigg\}
\end{aligned}
\tag{8.32}
$$

where

$F(x)$ = $2j\sqrt{x}e^{jx}\int_{\sqrt{x}}^{\infty} e^{-j\tau^2}d\tau$ is a Fresnel integral

$a^{\pm}(\phi'\pm\phi)$ = $2\cos^2\dfrac{2n\pi N^{\pm}-(\phi'\pm\phi)}{2}$

$N^{\pm}$ = integer that approximately satisfies equation $2n\pi N^{\pm}-(\phi'+\phi)=\pm\pi$ as close as possible

$\beta_0$ = angle between the incident ray and the edge of the wedge

$\phi$ = angle between the plane of diffraction and plane 0, as shown in Figure 8.16

$\phi'$ = angle between the plane of diffraction and plane 0, as shown in Figure 8.16

$k$ = wavenumber

$L$ = distance parameter dependent on the form of the incident wave for an incident spherical wave $L=\dfrac{ss'}{s+s'}\sin^2\beta_0$, and $s$ and $s'$ are distances from the diffracted point D to the source and observation point, respectively

$R_0^{\perp//}$ and $R_n^{\perp//}$ = reflection coefficients related to plane 0 with an incident angle $\phi$ and form a plane $n$ with a reflection angle $n\pi-\phi'$, respectively.

In a ray-fixed coordinate system, we have a relation similar to (8.31) for determining the diffracted fields. For an incident angle $\phi = 45°$ and $\beta = 90°$, the magnitude of the diffraction coefficients for a 90° concrete edge as a function of the diffraction angle at 1.8 GHz is shown in Figure 8.11. In our model, only the diffractions from the vertical corners of the walls that are recorded in the database are considered because most receivers and transmitters are generally vertically polarized. When a ray hits the edge, the edge is treated as a secondary source and all rays emanating from it are traced as a normal ray. Because the

strength of the diffracted ray is weak, the second- and higher-order diffraction effects are neglected.

*8.7.1.2 Improvement of the Computational Efficiency for 2D Ray Tracing.* A typical indoor environment is shown in Figure 8.12, where some furniture is present in the room. When applying a 2D ray-tracing algorithm, a database must be built. In order to deal with the differences in the dielectric properties among materials, each different object, such as a wooden door, a glass window, or a concrete wall, is defined as different regions. A boundary between any two regions is denoted by a line segment. All the data related to that segment, such as the point of origin, direction, length, thickness, and dielectric properties are specified. For example, there are 17 different segments for each sidewall of the corridor, and there are more than 80 segments in the environment of Figure 8.12.

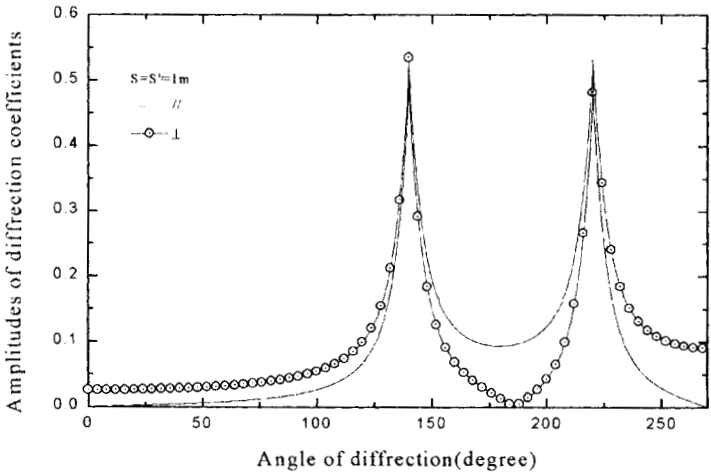


**Figure 8.11.** Magnitudes of the diffraction coefficients.

When a ray is traced through a usual 2D ray-tracing model, one needs to locate the ray intersections for every segment to determine whether there is an intersection. The equation for the ray is given by

$$\begin{cases} x = d_1 t + x_0 \\ y = d_2 t + y_0 \end{cases} \qquad (t \geq 0) \tag{8.33}$$

where $(x_0, y_0)$ is the origin and $(d_1, d_2)$ is the direction vector of the ray. The equation for a segment is given by

$$\begin{cases} x = a_1 m + x_1 \\ y = a_2 m + y_1 \end{cases} \qquad (0 \le m \le l) \tag{8.34}$$

where $(x_1, y_1)$ is the origin and $(a_1, a_2)$ are the direction cosines for each of the segments. The length of each segment is $L$. From (8.33) and (8.34), it is easy to obtain $t$ and $m$ and determine the point of intersection of the segments. From a geometrical point of view, one ray may intersect with many segments. It is important to get the point of intersection that is nearest the origin of the ray, where the reflection and refraction really occur.

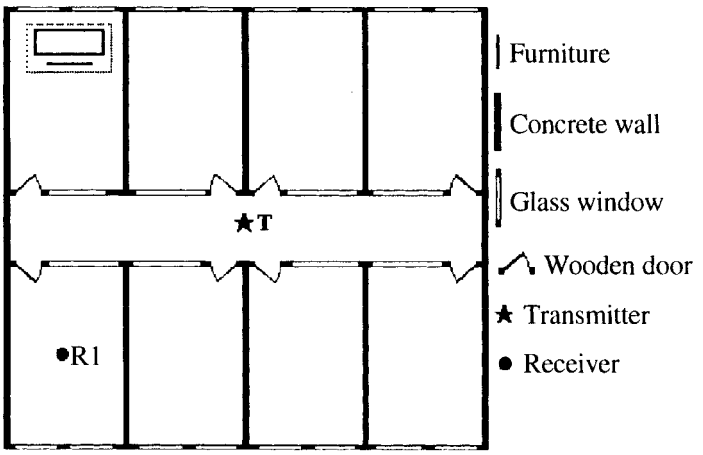


**Figure 8.12.** Typical environment for modeling propagation.

In fact, a ray usually intersects with only one segment before it changes its direction. This means that all computations of intersections with the remainder of the segments are not necessary. If all these computations are omitted, the computational efficiency of ray tracing will be greatly improved. In [133] the propagation area is divided into equal cells. But there are several disadvantages associated with this technique. It is difficult to determine the best size for the cell. Sometimes, there is no segment in a cell, and sometimes one segment crosses more than one cell. All these make the computations complicated. To overcome these difficulties, we have developed an irregular cell technique.

It is possible that physically disjoint segments of an indoor environment may lie on a straight line but are not continuous (e.g., open windows). We reorganize these segments into a line that can be described as a special segment without having any dielectric properties. According to this linear grouping method, the indoor environment as shown in Figure 8.12 has only nine lines. When there is furniture within the room, we can first introduce a rectangular box (indicated by a dashed line in Figure 8.12) to encompass it, and then consider the two

diagonals of the box as two virtual segments to see if the ray of interest intersects them. If the answer is yes, we take the real segments of the furniture into account; otherwise, we omit the entire box. That can result in considerable saving of the CPU time.

In our model we first build the database of segments of the indoor environment for prediction. All the segments in the database will be reorganized automatically into lines or boxes that form another database. When a 2D ray-tracing method is applied, only the intersections between rays and lines or boxes need to be determined. If a ray has no intersection with a line or two diagonals of a box, it has no intersection with the segment members of that line or box, and therefore tracing of the ray is terminated. For all the lines or boxes intersecting

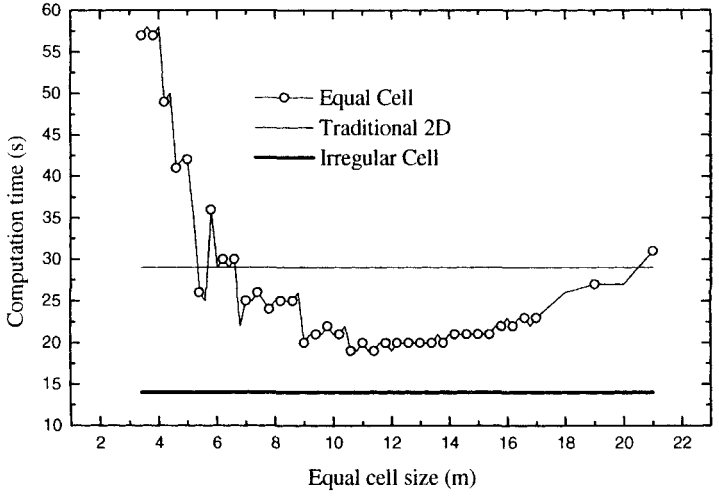


**Figure 8.13.** Computation time for predicting path loss at location R1 of Figure 8.12.

with the ray, the nearest line or box to the point of origin of the ray can be found and then the corresponding segments intersecting with the ray can also be determined. When the real intersecting segment is found, the electric field is calculated and both the reflected and refracted rays can be traced further.

In order to verify our model, numerical simulations have been carried out. The path losses in an indoor environment shown in Figure 8.12 have been predicted. The environment is composed of an area 17.9 $\times$ 20.8 $m^2$ and consists of concrete walls, wooden doors, glass windows, and furniture. The transmitter is located at the central part of the floor. The transmitting frequency is 1800 MHz. Figure 8.13 plots the computation time on a PC for calculating the path loss at the receiver location $R1$ as shown in Figure 8.12. It indicates that the proposed irregular cell method can save almost 60% of CPU time on the average over other traditional methods. The conclusion is also true for other locations of

transmitter and receivers in this environment. Because no ray intersections with objects have been omitted, the accuracy of the prediction does not degrade.

### *8.7.1.3 New Improved Model.*

• ***Patched-wall model.*** The layout for the measurement system shown in Figure 8.14 is on the 3rd floor of a building with many classrooms at Shanghai Jiao Tong University, Shanghai. In Figure 8.14, $T$ denotes the location of the transmitter and $R_n$ indicates the location of the receiver. The field is measured at 39 receiver locations. The width, length, and height of the floor are 18.26 m, 76.39 m, and 3.74 m, respectively. There are 20 rooms on this floor. The ceiling and the floor are made of concrete. The partition board between classrooms is

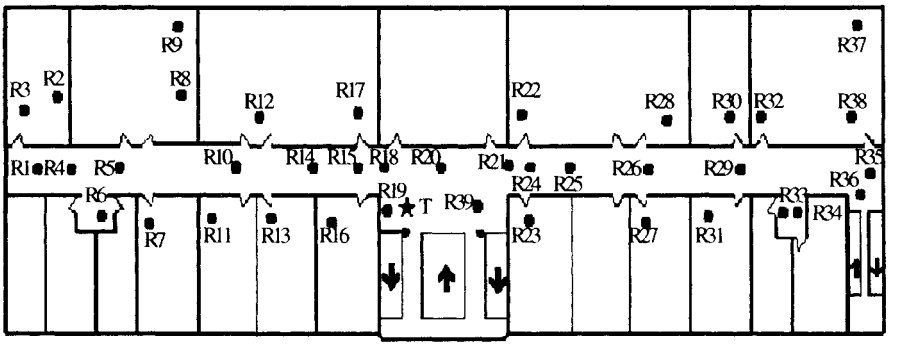


**Figure 8.14.** Layout of a building in the University (arrows mean stairs).

made of wood. The sidewalls of the corridor are mainly made of concrete. There are wooden doors and glass windows on these walls. Figure 8.15 shows a part of the sidewall. The front and back walls of the building are composed of concrete with inserts for glass windows.

Because of the differences in the dielectric characteristics between different materials, it is necessary to introduce patches of different dielectric constants and physical sizes to represent actual objects. Four different patches have been used. They are concrete walls, wooden doors, wooden partition boards, and glass windows. A database is built to record the location, thickness, and dielectric constants of all the patches. In order to simplify the calculation of the intersections, every patch is divided into several rectangles and is given an integer number for identification (ID). As shown in Figure 8.15, the patches are separated by dashed lines. There are 10 patches in Figure 8.15. The IDs of the patches having the same vertical projection on the floor are different only in the last digit. The ceiling and the floor are considered to be special patches. The measurement environment is divided into more than 400 patches that are stored in the database.

• ***Model description.*** The process of ray tracing is a complicated program of recursion. For the 3D model, there are many rays that need to be traced. But in fact, there are only a few rays that will reach the receiver. It is advantageous to search for the rays that will probably reach the receiver for tracing. In some simplified models, only singly reflected rays from the floor and ceiling are considered. Even though there may be no direct rays, however, multireflected rays from the floor and ceiling cannot be neglected.

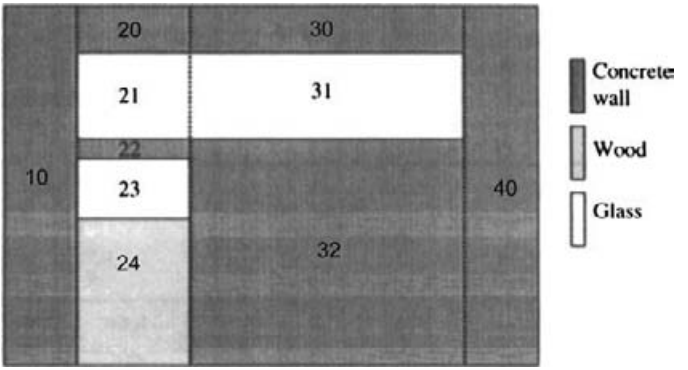


**Figure 8.15.** Part of an actual wall and how to divide it into patches.

Indoor environments are composed of floors, ceilings, and walls vertical to the floor. On a single floor (considering the floor to be the $x$–$y$ plane and the direction vertical to the floor the $z$-axis), one can find the following properties for propagation when using a ray-tracing technique. In this coordinate system, transmitter and receiver are regarded as points in a 3D space. Therefore:

1.) When the floor or the ceiling reflects a ray, the incident and reflected rays have the same azimuth angle. Namely, perpendicular projections of the two rays on the floor are in a line.
2.) When a wall vertical to the floor reflects a ray, the angle of incidence is equal to the angle of reflection along the perpendicular projection plane on the floor.
3.) The angle between the ray reflected by a wall and the $z$-axis is equal to that between the incident ray and the $z$-axis.
4.) Rays that have the same azimuth angle in a 3D space have the same perpendicular projection on the floor.

In our model, first we project all walls, objects, the transmitter, and the receiver (except the ceiling and the floor) vertically onto the floor and use a 2D ray-tracing technique on the projection plane and then apply a 3D ray-tracing

technique based on the results of a 2D ray tracing. This is explained through the following figures. Figure 8.16 characterizes a simple indoor environment with a wall, a ceiling, and a floor. The height of the transmitter and the receiver from the floor are $h_1$ and $h_2$, respectively. The height of the ceiling is $h$ above the floor. In Figure 8.17, the wall, the transmitter, and the receiver are projected vertically onto the floor. By performing a 2D ray tracing on the floor, one sees that there are only two paths from the projections of the transmitter and the receiver. If no reflection from the ceiling and the floor is considered, there are only two actual paths in the 3D space when using a 3D ray-tracing model. One is the direct path from the transmitter to the receiver; and the other includes one reflection from the wall.

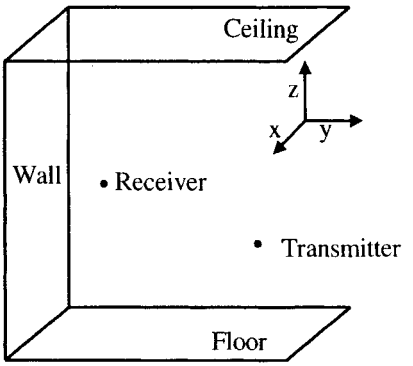


**Figure 8.16.** Simplified room structure.

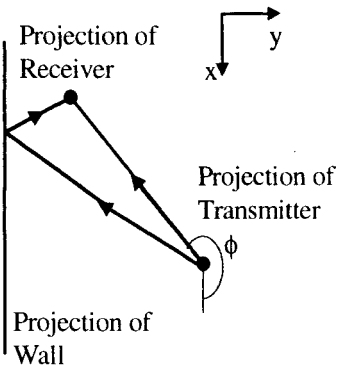


**Figure 8.17.** Projection onto the floor of various objects described in Figure 8.16.

When multiple reflections from the ceiling and floor are considered, the situation is different. We define the unfolded length of a path to be $d$ and the azimuth angle of the projection for the corresponding launching ray to be $\phi$. Using the properties of propagation, one can observe that rays launched in the 3D space that may reach the receiver is given by

$$\theta = \frac{\pi}{2} + \alpha \arctan \frac{2nh + \alpha h_0}{d} \tag{8.35}$$

where $h_0 = h_1 \pm h_2$, the positive sign is used when the total number of reflections from the ceiling and the floor is odd, and the negative sign is used when it is even, respectively. Possible values are $\alpha = \pm 1$. The positive value is used when the first reflection (does not include reflections from walls) occurs on the floor, and the negative value is used when it is from the ceiling.

These rays are all significant and should be launched in a 3D environment. The paths from the transmitter to the receiver for all these rays launched in 3D have the same perpendicular projection on the floor. The launching of the rays are carried out for $n = 0, 1, 2, \ldots, M$ ($n \neq 0$ when $\alpha = -1$), where $n$ is an index related to the order of reflection from the ceiling and the floor and $M$ is an index related to the maximum order of reflection from the ceiling and the floor. When $n = 0$, two 3D paths are included; one has no reflection from the ceiling or the floor, and the other has only one reflection from the floor. When $n = 1$, there are four 3D paths that are considered. The first path has one reflection from the ceiling. The second path has one reflection from the ceiling and then one reflection from the floor. The third one has one reflection from the floor and then one reflection from the ceiling, and the last one had one reflection from the floor, one reflection from the ceiling, and then one reflection from the floor again. So, the total number of useful 3D rays included in each 2D path is $2 + 4M$. The total 2D paths should include all reflections from all the walls.

During the 2D tracing on the projection plane, all 2D paths from the projection of the transmitter to the projection of the receiver are recorded and the unfolded length for each path is also calculated. After an integer $M$ is given, a 3D ray tracing is performed for all useful 3D launched rays corresponding to each 2D path. Because only parts of all 3D launching rays need to be traced, much time of computation can be saved. Based on Figure 8.17, Figure 8.18 shows the various paths in 3D space according to our model. If $M = 1$, then $n = 0$ and there are six paths in the 3D space corresponding to each 2D path as shown in Figure 8.17. Therefore, a total of 12 [$= 2 \times (2 + 4 \times 1)$] 3D rays are considered.

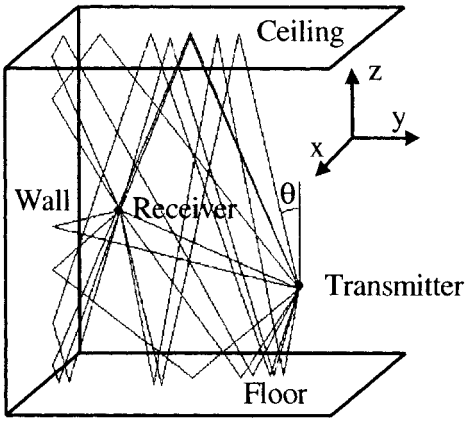


**Figure 8.18.** Tracing of rays in a three-dimensional space.

The field intensity of each ray is calculated using a 3D ray tracing. Finally, the total field intensity can be obtained by summing up all the individual field intensities. Our model includes direct, reflected, refracted, and diffracted fields that are represented by the rays. Each propagation mechanism is treated separately.

*8.7.1.4 Results of Simulation and Measurement.* The simulation environment and the measurement site are shown in Figure 8.14. In the prediction simulation, all the advantages of a 3D ray-tracing model have been taken into account in the new model. Because of the high computational efficiency of the 2D tracing technique, fewer useful 3D rays need to be traced. This 3D model just took 1% of the computation time over traditional 3D models. And because no useful rays have been ignored, the prediction accuracy is quite high.

To carry out the measurement, a 1.7-GHz narrowband CW signal generator is used as the transmitter. A 0- to 15-dBm CW signal is transmitted by a half-wavelength dipole antenna at a height of 1.6m above the floor. The signal is received by a half-wavelength dipole antenna located at a height of 1.5m from the floor. To assure that the propagation channel is stationary in time, the measured data has been averaged over 10 instantaneous sampled values.

Figure 8.19 shows both the predicted and measured results for the path loss at each location in the building. Predicted results from both the new model and the traditional 3D model have been presented along with measurements. However, the latter takes about 100 times more computation time than the new model. Because the position of receivers R18 and R19 are close to the transmitter, it is difficult to measure the path loss accurately. In the corridor, there is a LOS path or one reflected path so that the signal received at these locations is stronger than those inside the rooms.

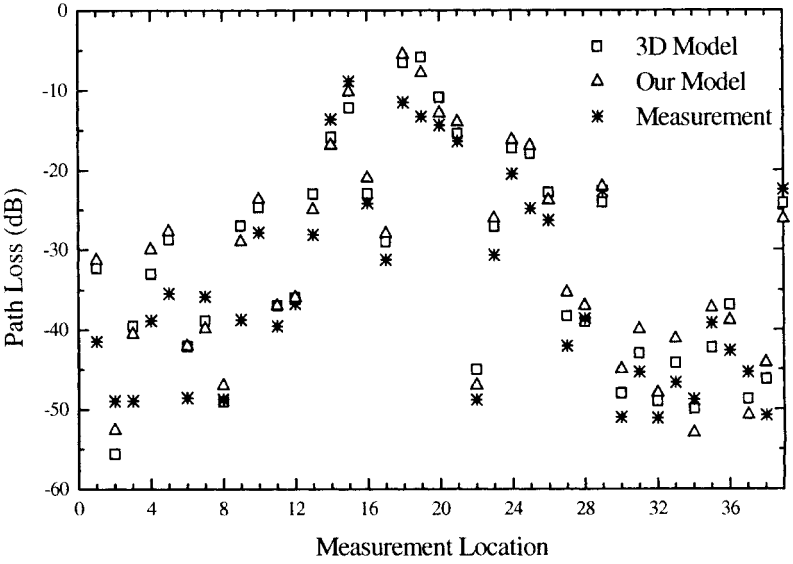


**Figure 8.19.** Results of simulation and measurement.

The method used in [61] has been extended to an indoor environment. In [61], the authors used the image method and projected objects on the ground to find an exact 3D path for an outdoor street scene. In this new model using multiple reflections from the floor and the ceiling and from one 2D path on a projection plane, many 3D paths can be determined. A formula to determine the 3D path has also been provided.

*8.7.1.5 Conclusion.* A computationally efficient method is described which transforms the results of a 2D ray-tracing method to a 3D model which has correlations with experimental results.

## 8.7.2. Analysis of the Effects of Walls on Indoor Wave Propagation Using FDTD

The ray-tracing technique does not take the effects of the inner structure of walls into account for indoor propagation prediction. A numerical approach to treat this problem using the FDTD method is now described. Numerical results for path loss calculated by a FDTD method are compared with those obtained by the ray-tracing technique. Use of a ray-tracing technique in propagation prediction has been under development for more than a decade. It is powerful and easy to use.

There have been a number of recent investigations on indoor radio propagation modeling using a ray-tracing method [57, 65, 126], but few pay attention to the inner structure of the walls [134, 135]. When using a ray-tracing method, it is assumed that reflection from walls has a substantial specular component. Typical concrete blocks used in wall construction are shown in Figure.8.20. The air hole in the block forms a periodicity of blocks. It is found that nonspecular reflection occurs when the operating frequency is above 1.2 GHz [134].

In this approach, the reflection and transmission characteristics of the walls can be derived by solving for higher-order Floquet modes. Also, the method of homogenization can be used to determine the effective material properties of walls, but they did not consider nonspecular reflection.

In this section, the FDTD method is used to predict propagation properties for indoor environments [137]. The periodic structure of walls is also considered. Numerical results for the path loss are calculated by a FDTD method and are compared to those obtained by the ray-tracing method. It is proved that the inner structure of walls has a considerable influence on the path loss when predicting propagation, and the FDTD method can give more accurate results.

In this approach, the reflection and transmission characteristics of the walls can be derived by solving for higher-order Floquet modes. Also, the method of homogenization can be used to determine the effective material properties of walls, but they did not consider nonspecular reflection.

In this section, the FDTD method is used to predict propagation properties for indoor environments [137]. The periodic structure of walls is also considered. Numerical results for the path loss is calculated by a FDTD method and are compared to those obtained by the ray-tracing method. It is proved that the inner structure of walls has a considerable influence on the path loss when predicting propagation, and the FDTD method can give more accurate results.

*8.7.2.1* ***Description of the Procedure.*** For the analysis of a wall at a frequency of 1.8 GHz, the parameters for the model of Figure 8.20 are chosen as $d = \lambda_0/20$ and the relative dielectric constants of a concrete wall as $\varepsilon_r = 3$. When a plane wave in the $x$–$z$ plane is incident on the layered periodic structure at an angle $\theta$ to the $z$-axis with an electric field polarized along $y$, the inner periodic layer of the structure will support an infinite set of modes with different wavenumbers, $km$ ($m = 0, \pm1, \pm2, \ldots$). The field produced by these modes can in turn be decomposed into a series of space harmonics ($n = 0, \pm1, \pm2, \ldots$), each having a wavenumber $\beta_n = k_0 \sin\theta + 2\pi n/T$ along $x$, where $k_0$ is the wavenumber of the incident wave in free space and $T$ is the period of the inner structure. The space harmonics in the periodic region will couple to the air region. As a result, there will exist reflected and transmitted space harmonics whose directions of propagation in the air are given by $\sin\phi_n = \beta_n/k_0$, where $\phi_n$ is the outbound angle relative to the normal [134]. At higher frequencies, more modes have real $\phi_n$ and will carry power along nonspecular directions. Figure 8.21 shows the relation of the incident angle and the outbound angle for the structure of Figure 8.20 at 1.8 GHz when $n = 0, \pm1$.

In order to observe the effects of the inner structure of the walls on wave propagation, consider a room with a wooden door, glass windows, and concrete walls which are placed in the computation area as shown in Figure 8.22. A two-dimensional FDTD method is applied. An artificial outer boundary encloses the room defining the computational area. A second-order radiation boundary condition has been used at the outer boundary. The incremental spatial step is d and the time step is $d/(2C)$, where $C$ is the wave velocity in free space. The thickness of the wooden door, which has a permittivity of $\varepsilon_r = 1.9$, is $6d$. The thickness of the glass windows is $d$ and it has a permittivity of $\varepsilon_r = 3.9$. A line source ($T$) to simulate the antenna is placed outside the room. A CW signal with an electric field polarized along the $y$-axis is transmitted at 1.8 GHz. The path loss at 250 points from left to right along a line is evaluated and compared with the results of ray tracing. When using the ray-tracing method, the transmitter is treated as a point source.

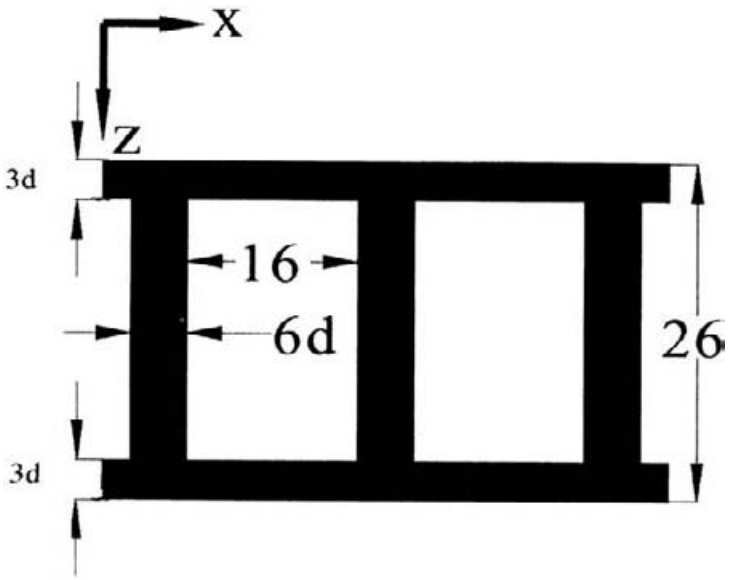


**Figure 8.20.** Typical periodic inner structure of the walls.

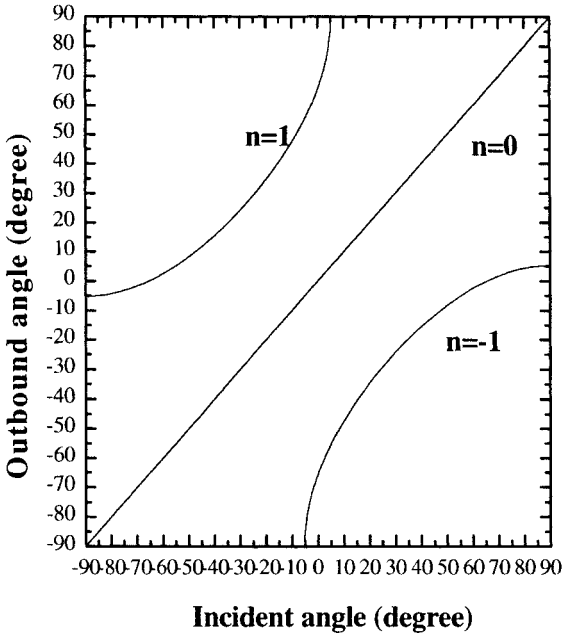


**Figure 8.21.** Outbound angle (in degrees) of the $n = 0, \pm 1$ space harmonic modes as a function of the incident angle (in degrees).

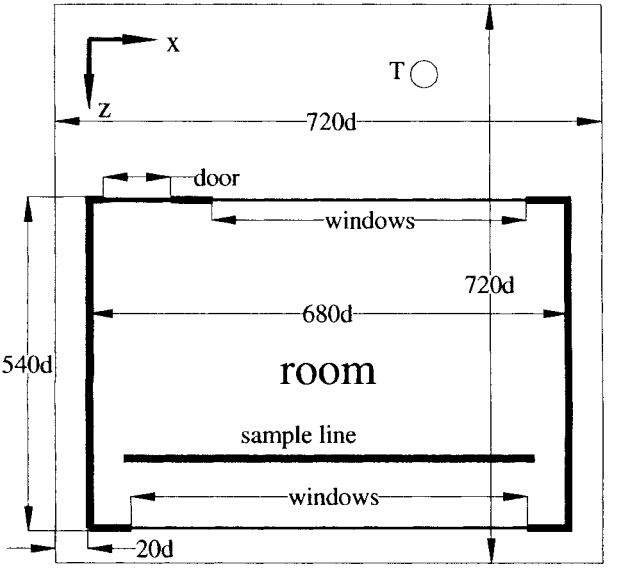


**Figure 8.22.** Two-dimensional geometry of the grid for the FDTD method.

*8.7.2.2* ***Numerical Results.*** The fields of the environment are calculated using a 2D FDTD method when the wall is (1) assumed to be a periodic structure, and (2) uniform in nature with an effective dielectric constant. For the FDTD method, 5000 time steps are calculated and it takes more than 6 hours of CPU time on a PC. A 2D ray-tracing method is used to analyze the uniform structure, and it takes only 10 minutes to compute the path loss for 250 sample points.

Figure 8.23 shows the simulation results of path loss for the sample points. It indicates that the effects of the inner structure of the walls cannot be neglected for propagation prediction. The maximum difference in field strength when the wave is assumed to propagate through a periodic structure and a uniform structure is more than 10 dB when using the FDTD method. As a full-wave analysis tool, FDTD is more accurate than the ray-tracing method. All the propagation phenomena, such as reflection, transmission, and diffraction, are included. A ray-tracing method considers only reflection and transmission. The maximum difference in the field strength when propagating through a periodic structure using the FDTD method and the ray-tracing method is around 18 dB.

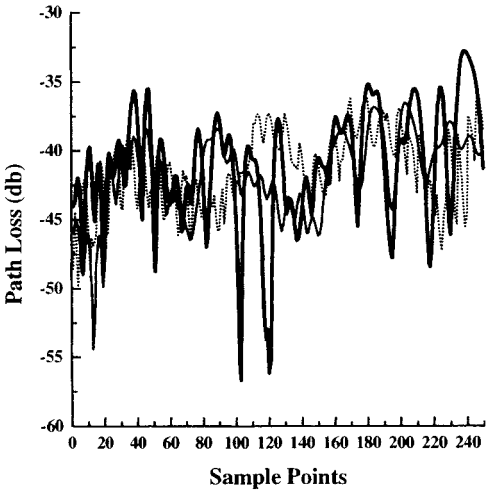


**Figure 8.23.** Simulation results using three different FDTD methods.
▬▬, FDTD (periodic); ———, FDTD (uniform); -------, ray tracing (uniform).

## 8.8 MODELS FOR SMALL-SCALE FADING

*Small-scale fading* refers to dramatic changes in signal amplitude and phase that can be experienced as a result of small changes (as small as a half-wavelength) in the spatial separation between a receiver and a transmitter. These changes in the

envelope of the received signal is statistically described by a stochastic process.

In order to get a sound understanding of the channel, it is important to study the distribution of the envelope of the received signal. A few possible choices of the statistical distributions to model the envelope are explained below. As explained and emphasized in Appendix A, we have to be extremely careful when using a statistical model, as a complete lack of knowledge of the system cannot be supplemented by a stochastical distribution.

### 8.8.1 Ricean Distribution

When there is a dominant stationary (nonfading) signal component present, such as a line-of-sight propagation path, the fading distribution is Ricean. The Ricean distribution (also called *Rice distribution* or *Rician distribution*) is given by

$$p(r)=\begin{cases}\dfrac{r}{\sigma}\exp\left[\dfrac{r^2+Ar}{2\sigma^2}\right]I_0\left(\dfrac{Ar}{\sigma^2}\right) & (A\geq 0,\ r\geq 0)\\ 0 & r<0\end{cases} \tag{8.36}$$

where $r$ is the amplitude of the envelope of the received signal, $2\sigma^2$ is the predicted mean power of the multipath signal, $A$ denotes the peak amplitude of the dominant signal, and $I_0(\bullet)$ is the modified Bessel function of the first kind and zero order. The Ricean distribution is often described in terms of a parameter $K$, which is defined as the ratio between the deterministic signal power and the variance of the multipath. It is given by [10]

$$K(dB)=10\log\frac{A^2}{2\sigma^2} \tag{8.37}$$

$K$ is known as the *Ricean factor* and completely specifies the distribution.

It is possible to estimate the Ricean $K$-factor of a signal, from measurements of received power versus time. One approach is to compute the distributions of the measured data, then compare the result to a set of hypothesis distributions using a suitable goodness-of-fit test. Another is to compute a maximum likelihood estimate using an expectation/maximization (EM) algorithm. However, both of these approaches are relatively cumbersome and time consuming. A simple and rapid method has been developed based on calculating the first and second moments of the time series data. When perfect moment estimates of the Ricean envelopes are available, the method is exact. In that case, the factor $K$ can only be obtained implicitly, by equating a ratio of the measured moments to a complicated function of $K$. By contrast, the method described in [89] yields an explicit and quite simple expression for $K$ in terms of the measured moments.

### 8.8.2 Rayleigh Distribution

As the dominant signal in Ricean distribution becomes weaker, the composite signal resembles a noise signal which has the envelope of a Rayleigh distribution. For mobile radio channels, the Rayleigh distribution is widely used to describe the statistical time-varying nature of the received envelope of a flat fading signal, or an individual multipath component. The Rayleigh distribution has a probability density function (pdf) given by

$$p(r)=\begin{cases}\dfrac{r}{\sigma^2}\exp\left(-\dfrac{r^2}{2\sigma^2}\right) & (0\le r\le\infty \\ 0 & (r<0)\end{cases} \tag{8.38}$$

The probability that the envelope of the received signal does not exceed a specified value $R$ is given by the corresponding cumulative distribution function (cdf):

$$P(R) = P_r(r<R) = \int_0^R p(r)dr = 1-\exp\left(-\frac{R^2}{2\sigma^2}\right) \tag{8.39}$$

where $r$ is the envelope amplitude of the received signal and $2\sigma^2$ is the predicted mean power of the multipath signal.

Since the fading data are usually measured in terms of the fields, quantities for a particular distribution cannot be assumed. The median value is often used other than the mean values and it is easy to compare different fading distributions which may have widely varying means. A typical Rayleigh fading envelope for a moving mobile at 900 MHz is shown in Figure 8.24 [90].

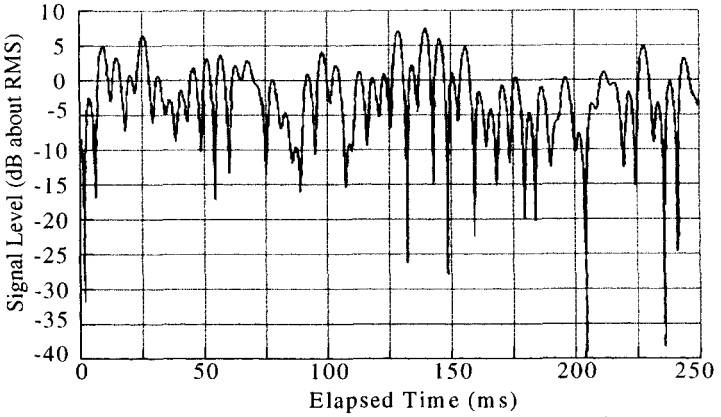


**Figure 8.24.** Typical Rayleigh fading envelope at 900 MHz received by a mobile traveling at 120 km/hr.

### 8.8.3 Lognormal Fading Model

The lognormal fading model is quantified to represent the distribution of rays which experience multiple reflections and diffractions between a transmitter and a receiver. The lognormal pdf can be expressed as

$$p(r) = \frac{1}{r\sqrt{2\pi\sigma^2}} \exp\left\{ - \frac{[\ell n(r) - m]^2}{2\sigma^2} \right\} \tag{8.40}$$

where $m$ is the median value and $\sigma$ is the standard deviation of the corresponding normal distribution, obtained by using the transformation $y = \ell n(r)$ [91]. Techniques such as the Monte Carlo method and Schwartz and Yeh method have been developed to simulate the power sum for the lognormal components [92].

### 8.8.4 Suzuki Model

The Suzuki model combines the lognormal and Rayleigh distributions and provides a more accurate approximation of the sum of correlated complex lognormals for a wider variety of channel behaviors. Usually, the Rayleigh distribution is obtained from two statistical independent normal processes, $\mu_1(t)$ and $\mu_2(t)$, with zero means and identical autocorrelation functions according to the relation

$$\xi(t) = \sqrt{\mu_1^2(t) + \mu_2^2(t)} \tag{8.41}$$

where $\xi(t)$ can be regarded as the envelope of one complex-valued normal random process $\lambda$(t). The requirement of statistical independence between $\mu_1(t)$ and $\mu_2(t)$ is identical with the demand for a symmetrical power spectrum for $\lambda(t)$. The received power averaged over a period of a few seconds can vary considerably due to various shadowing effects. In order to adapt the model to this behavior, the process $\xi(t)$ is substituted by the product $\eta(t) = \zeta(t) \times \xi(r)$, where the lognormal process $\zeta(t) = \exp[\mu_3(t)]$ is defined by a normal process $\mu_3(t)$ with variance $s^2$ and mean $m$. The product process with this particular amplitude density distribution is called the *Suzuki process* and is given by [93]

$$p_\eta(r) = \int_0^\infty \frac{r}{\sigma^2} \exp\left( \frac{r^2}{2\sigma} \right) \frac{1}{\sqrt{2\pi}\, s\sigma} \exp\left[ - \frac{(\ell n\sigma - m)^2}{2s^2} \right] d\sigma \tag{8.42}$$

where $\sigma$ is the standard deviation and $r$ is the amplitude. The assumption of statistical independence does not always meet the real conditions in a multipath wave propagation, so it has been modified [94] and simulated in [95].

It is a widely accepted statistical model for the received signal envelope in macrocellular mobile radio channels, where there is no direct LOS path.

### 8.8.5 Nakagami Model

The Nakagami Model was developed in the early 1940s. The corresponding probability density function is written as [96]

$$p(r) = \frac{2m^m r^{2m-1} \exp\left(-\frac{m}{\Omega} r^2\right)}{\Gamma(m)\,\Omega^m} \tag{8.43}$$

Here, $r$ is the envelope amplitude of the received signal, $\Omega = < r^2 >$ is the time-averaged power of the received signal, and $m = < r^2 >^2 / < (r^2 - < r >^2)^2 >$ is the inverse of the normalized variance of $r^2$. $\Gamma(\bullet)$ is the Gamma function. The Nakagami pdf may be shown to be a more general expression of other well-known density functions. For $m = 1$, the Rayleigh probability density function is obtained. It can also be approximated by both Rice and lognormal distributions over certain domains given the appropriate bounds on the parameters.

A Nakagami model parameterized by the fading severity parameter $m$ has been shown to fit well to some urban multipath propagation data. A simulation of the Nakagami model has been presented in [97].

### 8.8.6 Weibull Model

The Weibull model arises when results from mobile radio propagation measurements are plotted on graph paper that is scaled such that a Rayleigh distribution appears as a straight line with a slope of −1. The Weibull pdf can be written as [91]

$$p(r) = \frac{\alpha b}{r_0}\left(\frac{br}{r_0}\right)^{\alpha-1} \exp\left[-\left(\frac{br}{r_0}\right)^{\alpha}\right] \tag{8.44}$$

where $\alpha$ is a shape parameter, which is chosen so as to yield a best fit to the measurement results. $r_0$ is the RMS value for $r$. $b = \sqrt{(2/\alpha)\Gamma(2/\alpha)}$ is a normalization factor. For the special case in which $\alpha = 1/2$, it becomes a Rayleigh pdf. The Weibull distribution provides flexibility to model any shape offered by a Nakagami distribution, but it lacks a theoretical basis. In [146] it is shown that the Weibull distribution characterizes indoor propagation path losses quite well.

### 8.8.7 Other Fading Models

Many other models for fading have been developed. They are the *Rice-lognormal model* [98], *Nakagam–Rice model* [99], *Nakagami-lognormal model* [100], and the *K*-distribution, which is a substitute for the *Rayleigh-lognormal distribution* [101]. They are mixtures of two kinds of distributions and are now widely used. In [102], propagation models that include both the effects of shadowing and multipath fading have been developed and have been used in studying terrestrial and satellite channels. In [103, 104] a new theoretical model for the prediction of fast fading in an indoor environment has been developed. This model makes the assumption that the number of dominant propagation paths that contribute to the signal in the receiver in a multipath environment is not infinite but rather small (e.g., 15). This assumption leads to the development of a new theoretical model called POCA that is more general and more efficient than the Rayleigh one, especially for indoor environments, and it fits generally for environments in which a small number of dominant propagation paths exist.

In this section, some of the statistical models for fading have been introduced. Only their pdf distribution has been described. Details of the implementation of these models can be obtained from the various references cited.

## 8.9 IMPULSE RESPONSE MODELS

Narrowband or continuous wave (CW) path loss is a parameter that can predict the power level of the system and the space coverage of a base station. In modern mobile communication systems with high data rates and small cell size it is necessary to model the effects of multipath delay as well as fading. The impulse response is a useful characterization of the system since the output of the system can be computed through convolution of the input with the impulse response if the system is linear. A multipath propagation channel is modeled as a linear filter and has a complex baseband impulse response [105–125, 144, 147–151].

In digital wireless communications, one of the main reasons of occurrence of bit errors is intersymbol interference (ISI) caused by multipath propagation. If the symbol rate is much lower than the coherent bandwidth, time delay spread can be neglected. In this case, multipath propagation only causes fading of the signal level, and Gaussian noise is the dominant factor that causes bit errors. If the symbol rate is relatively high, time delay spread cannot be neglected.

A large number of measurements have been made for the impulse response for both outdoor and indoor environments. Based on the measured data, some models have been derived. The results of measurements along with some typical models are described here followed by some deterministic models.

### 8.9.1 Models Based on Measurement Results

Because of the importance of determining the time delay spread for wireless communications, a number of wideband channel sounding techniques have been developed. These techniques may be classified as: (1) direct pulse measurements, (2) spread spectrum sliding correlator measurement, and (3) swept frequency measurements.

The block diagram for each of these techniques is shown in Figure 8.25 [10]. Almost the same result can be obtained from the last two methods [105]. Some measurements, both for indoor and outdoor environments and the calculated RMS time delay, have been summarized in Table 8.5, where Med indicates median values, T-R indicates the distance between transmitter and receiver, and Ave. implies the mean average values. In Table 8.5 it is found that the RMS delay spread varies from several nanoseconds to several microseconds, corresponding to different environments and frequencies.

There are many factors affecting the impulse response, such as frequency, height of transmitting and receiving antennas, fixed objects (mountains, buildings, or indoor furniture), and moving humans or objects close to the transmitter and/or the receiver. It is shown in Table 8.5 that the RMS time delay varies little for different frequencies for indoor environments [106], but a different conclusion has been obtained in [107]. In [108] it is found that at 11.5 GHz, RMS time delay in most cases is significantly smaller than at 2.4 GHz and 4.75 GHz, which are in general about the same. The reason that two different conclusions have been reached is that all these various conjectures have been derived from specific measurements. OLOS (obstructed line-of-sight) channels are subjected to higher variations in RMS delay spread caused by movement of the terminal around a small area because of the presence of more scatters in OLOS than in an LOS environment. On the other hand, the short time variations in the RMS delay spread in OLOS environments are found to be less than those in LOS environments [117]. It is concluded that in an empty indoor environment the RMS delay spread is a function of transmit-receive separation, and when there are furniture and mazes of semipermanent partitions, RMS delay spread becomes constant for all ranges [105]. It is shown in [121] that in many cities where terrain is flat, RMS delay spreads do not exceed 7 or 8 μs, and in urban areas with surrounding hills, RMS delay spreads do not exceed 13.5 μs. In [26, 123], RMS delay spread has been analyzed as a function of path loss and the height of antenna. The predicted results may be bounded by an exponential model of the form $\tau_{RMS}(ns) = \exp(0.065PL)$, where PL is the path loss in decibels. Table 8.6 shows the measurements of $\tau_{RMS}$ with relation to the height of the antennas. It indicates that the delay spread increases as the antenna height increases because as the antenna is raised it becomes visible to more objects scattering the electromagnetic radiation at greater distances.

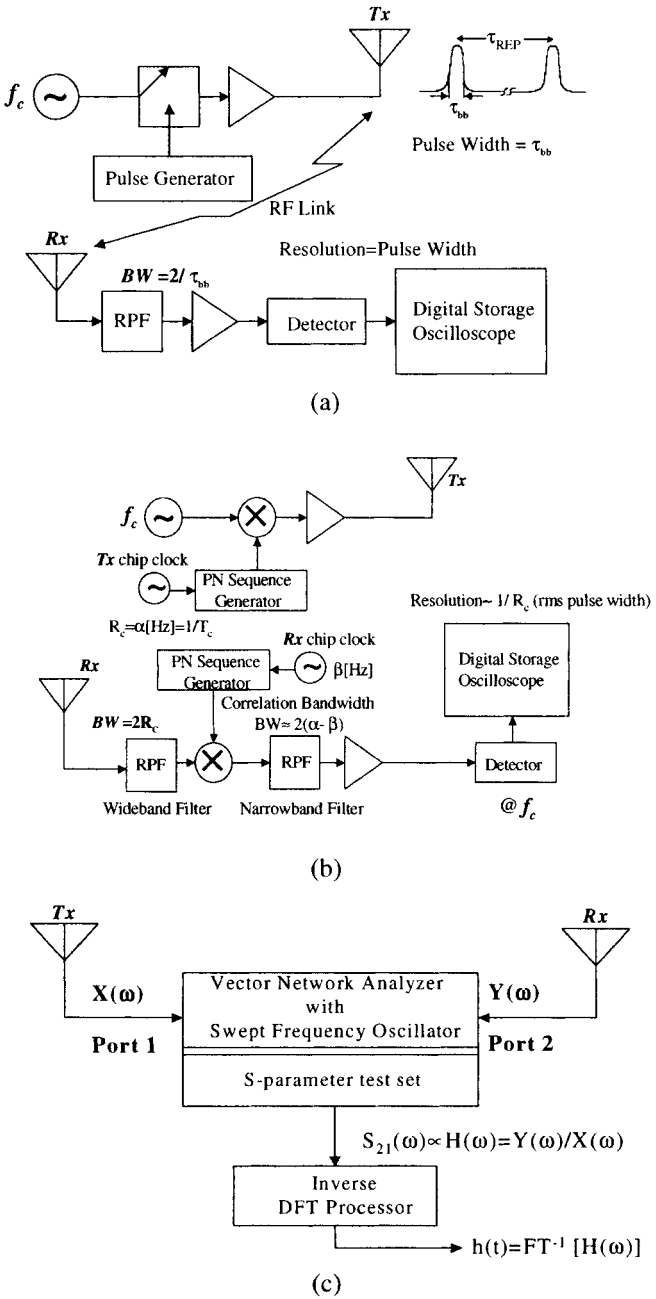


**Figure 8.25.** Block diagrams of the impulse response measurement system: (a) direct RF channel impulse response measurement system; (b) spread spectrum channel impulse measurement system; (c) frequency domain channel impulse measurement.

**TABLE 8.5**
Measurements and RMS delay spreads

| Technique | Location | $\tau_{RMS}$(ns) | Frequency (MHz) | Reference |
|---|---|---|---|---|
| B | Office building | 30–100 | 850, 1,700 | [106] |
| A | Manufacturing floors | 15–29(Area A)<br>31–62(Area B)<br>48–90(Area C)<br>52–57(Area D)<br>19–37(Area E) | 910 | [109] |
| A | Indoor sports arena<br>Open-plan factory<br>Textile plant<br>Office building | 7–120<br>40–30<br>15–125<br>5–40 | 1,300<br>4,000 | [110] |
| A | Within a room<br>(4 rooms) | 7–16<br>10 ns(Med.) | 37,200 | [111] |
| B | Urban area I<br><br>Urban area II | 98–1270<br>590(Ave.)<br>61–2940<br>480(Ave.) | 910 | [111][112] |
| C | Building 1<br>Building 2 | About 12–72<br>About 4–25 | 40,000 | [113] |
| B | Sidewalk of LOS street | 0.5d + 40<br>(*d* is T-R) | 2,600 | [113][114] |
| A | Engineering bldg.<br>Retail store | 12.85–84.60<br>20.74–102.44 | 2,400 | [115] |
| – | Laboratories at same floor | 8.3 LOS (Med.)<br>14.1 OLOS1 (Med.)<br>22.3 OLOS2 (Med.) | 910 | [117] |
| B | Outdoor Site1<br>Site2<br>Site 3 | 60–250, 130(Med.)<br>40–130, 70(Med.)<br>60–250, 120(Med.) | – | [118] |
| C | In two buildings | 10–50 with<br>mean 20–30 | 900–1300 | [119] |
| C | Four types of indoor locations | 10–20 (Med.)<br>10–20 (Med.)<br>5–15 (Med.) | 2,400<br>4,750<br>1,150 | [108] |
| A | Hamburg<br>Dusseldorf<br>Frankfurt (bank)<br>Frankfurt (apart.) | 1300 (typical)<br>3100 (typical)<br>8100 (largest)<br>19,600 (largest) | 942.225 | [120] |
| A | Washington<br>Greenbelt<br>Oakland<br>San Francisco | 2500–7500<br>2000–7000<br>2500–13,500<br>1000–25,500 | 892 | [121] |
| – | LOS (100–400m) | 140.6–325.4 | 2,197.5 | [122] |

**TABLE 8.6**
RMS delay spread as a function of the height of an antenna

| Antenna Height | Mean RMS Delay (ns) | Standard Deviation of RMS Delay (ns) | Location | Reference |
|---|---|---|---|---|
| 3.7 m | 136.8 | 138.0 | San Francisco | [26] |
| 8.5 m | 176.8 | 147.1 | | |
| 13.3 m | 275.9 | 352.0 | | |
| 3.7 m | 134.6 | 127.4 | Ottawa | [123] |
| 8.5 m | 173.1 | 156.8 | | |

### 8.9.2 Statistical Models of Time Delay Spread

*8.9.2.1 Two-ray Rayleigh Fading Model.* A commonly used multipath model is an independent Rayleigh fading two-ray model [10]. The impulse response of the model is represented by

$$h(t) = \alpha_1 \exp[j\theta_1(t)]\delta(t) + \alpha_2 \exp[j\theta_2(t)]\,\delta(t-\tau) \tag{8.45}$$

where $\alpha_1$ and $\alpha_2$ are independent random variables and have a Rayleigh pdf. $\theta_1$ and $\theta_2$ are also two independent random variables and their density functions are uniformly distributed over $[0, 2\pi]$. $\tau$ is the time delay between the two rays.

*8.9.2.2 Saleh and Valenzuela Model.* Saleh and Valenzuela [30] reported the results of indoor measurements between two vertically polarized omni-directional antennas located on the same floor of a medium-sized office building. The measurements indicate that the statistics of the channel impulse response are independent of the polarizations of the transmitting and receiving antennas if there is no line-of-sight path between them. The model assumes that the multipath components arrive in clusters. The clusters and components within a cluster form a Poisson arrival process with different rates.

*8.9.2.3 Lognormal At Any distance.* In [124], Cardoso and Mouliness present three conjectures about delay spread. The first is that $\tau_{\text{RMS}}$ is lognormal at any distance. This is derived from measurement data which are classified into urban, suburban, rural, and mountainous area. The second conjecture is that the median $\tau_{\text{RMS}}$ increases with distance, and the third conjecture is that $\tau_{\text{RMS}}$ tends to increase with shadow fading. $\tau_{\text{RMS}}$ can be given by

$$\tau_{\text{RMS}} = T_1 d^{\varepsilon} y \tag{8.46}$$

where $T_1$ is the median value of $\tau_{\text{RMS}}$ at $d = 1$ *km*, $\varepsilon$, is an exponent that lies between 0.5–1.0, and $y$ is the lognormal variate.

*8.9.2.4 SIRCIM Model.* Based on measurements at 1300 MHz in five factory and other types of buildings, the piecewise functions of excess delay for the probabilities of multipath arrivals are derived as [3]:

$$P_R(T_K, S_1) = \begin{cases} 1 - \dfrac{T_K}{367} & T_K < 110\,\text{ns} \\ 0.65 - \dfrac{T_K - 110}{360} & 110\,\text{ns} < T_K < 200\,\text{ns} \\ 0.22 - \dfrac{T_K - 200}{1360} & 200\,\text{ns} < T_K < 500\,\text{ns} \end{cases} \tag{8.47}$$

$$P_R(T_K, S_2) = \begin{cases} 0.55 + \dfrac{T_K}{667} & T_K < 100\,\text{ns} \\ 0.08 + 0.62e^{-\frac{T_K - 100}{75}} & 100\,\text{ns} < T_K < 500\,\text{ns} \end{cases} \tag{8.48}$$

where $S_1$ and $S_2$ correspond to LOS and OLOS environments, respectively. $T_K$ in units of nanoseconds is the excess delay at which a multipath component will arrive at the receiver and takes on values which are integer multiples of 7.8 ns.

*8.9.2.5 Δ–K Model.* This model [9, 119] takes into account the clustering property of paths caused by the grouping property of scatterers. The process is described by transitions between two states representing different mean arrival rates. Initially, the process starts in state 1 with a mean arrival rate $\lambda_0(t)$. If a path arrives at time $t$, transition is made to state 2 with a mean arrival rate $K\lambda_0(t)$. If no additional paths arrive in the interval $[t, t + \Delta]$, a transition is made back to State 1 at the end of the interval.

*8.9.2.6 Discrete-Time Model.* In this model [119, 125], the time axis is divided into small time intervals called bins. Each bin is assumed to contain either one multipath component or no multipath component. The possibility of more than one path in a bin is excluded. A reasonable bin size is the resolution of the specific measurement.

### 8.9.3 Deterministic Models of Time Delay Spread

The statistical models above are based on measurements made in a specific environment. It may not be suitable for prediction in other environments.

*8.9.3.1 Ray Tracing.* In theory, ray-tracing technique [12, 105, 118, 123, 127] can determine almost all multipath components, including their amplitude, time delay, and phase, and it is effective in predicting the time delay spread. When applying a ray tracing method, detailed knowledge of the environment is required. Another advantage of ray-tracing models over other propagation models is its ability to incorporate antenna radiation patterns and particularly to consider the effect of the radiation pattern on each ray individually.

Since the phase of each ray arriving at a receiver varies significantly with distance and cannot be accurately predicted, it will be impossible to achieve agreement with either the instantaneous measured shape or the value of the RMS delay spread for a single individual measurement. The comparison between measured and modeled results should be for average values in a small area around the actual mobile position [127]. A seven-ray and a 25-ray model consider only single or double reflections, respectively, and are used to simulate propagation in a room [105]. The RMS delay spread is predicted and agrees well with that calculated from measurements.

*8.9.3.2 VRP Model.* This model is similar to a seven-ray model but in an outdoor environment. It assumes some virtual reflection points (VRPs) located at the intersection points along the LOS on streets and at building walls [122]. It does not consider the effects of traffic and moving human. The predicted results of the *RMS* delay spreads are verified by measurements.

## 8.10 CONCLUSION

Propagation models are not only needed for installation guidelines, but also play a key part of any analysis or design that strives to mitigate interference. In this chapter we have surveyed some of the typical propagation models which provide good estimates for both large- and small-scale fading channels. Despite the enormous efforts to date, much work remains in the understanding and predicting the characters of mobile communications channels. In addition, an efficient ray-tracing method has been presented for tracing rays in an indoor propagation system. A FDTD method has been described to analyze wave propagation through the walls in a building.

## REFERENCES

[1] H. L. Bertoni, *Radio Propagation for Modern Wireless Systems*, Prentice Hall, Upper Saddle River, NJ, pp. 90–92, 2000.

[2] J. B. Andersen, T. S. Rappaport, and S. Yoshida, "Propagation Measurement and Models for Wireless Communications Channels," *IEEE Communications Magazine*, Vol. 33, No. 1, pp. 42–49, Jan. 1995.

[3] T. S. Rappaport, S. Y. Seidel, and K. Takamizawa, "Statistical Channel Impulse Response Models for Factory and Open Plan Building Radio Communicate System Design," *IEEE Transactions on Communications*, Vol. 39, No. 5, pp. 794–807, May 1991.

[4] W. C. Y. Lee, *Mobile Cellular Telecommunications Systems*, McGraw-Hill, New York, 1989.

[5] B. Sklar, "Rayleigh Fading Channels in Mobile Digital Communication Systems, Part I," *IEEE Communications Magazine*, Vol. 35, No. 9, pp. 136–146, 1997.

[6] L. C. Godara, "Applications of Antenna Arrays to Mobile Communications, Part I, Performance Improvement, Feasibility, and System Considerations," *Proceedings of the IEEE*, Vol. 85, No. 7, pp. 1031–1060, July 1997.

[7] M. Chryssomallis, "Smart Antennas," *IEEE Antennas and Propagation Magazine*, Vol. 42, No. 3, pp. 129–136, June 2000.

[8] G. G. Raleigh and T. Boros, "Joint Space–time Parameter Estimation for Wireless Communication Channels," *IEEE Transactions on Signal Processing*, Vol. 46, No. 5, pp. 1333–1343, May 1998.

[9] G. L. Turin, "A Statistical Model for Urban Multipath Propagation," *IEEE Transactions on Vehicular Technology*, Vol. 21, No. 1, pp. 1–9, 1972.

[10] T. S. Rappaport, *Wireless Communications: Principles and Practice*, Prentice Hall, Upper Saddle River, NJ, 1996.

[11] M. F. Catedra, J. Perez, F. Saez de Adana, and O. Gutierrez, "Efficient Ray-Tracing Techniques for Three Dimensional Analyses of Propagation in Mobile Communications: Application to Picocell and Microcell Scenarios," *IEEE Antennas and Propagation Magazine*, Vol. 40, No. 2, pp. 15–27, Apr. 1998.

[12] S. Y. Seidel and T. S. Rappaport, "Site-Specific Propagation Prediction for Wireless In-Building Personal Communication System Design," *IEEE Transactions on Vehicular Technology*, Vol. 43, No. 4, pp. 879–891, 1994.

[13] D. Molkdar, "Review on Radio Propagation into and within Buildings," *IEE Proceedings H*, Vol. 138, No. 1, pp. 61–73, Feb. 1991.

[14] T. Okumura, E. Ohmori, and K. Fukuda, "Field Strength and Its Variability in VHF and UHF Land Mobile Service," *Review Electrical Communication Laboratory*, Vol. 16, No. 9–10, pp. 825–873, 1968.

[15] M. Hata, "Empirical Formula for Propagation Loss in Land Mobile Radio Service," *IEEE Transactions on Vehicular Technology*, Vol. 29, No. 3, pp. 317–325, 1980.

[16] J. Walfisch and H. L. Bertoni, "A Theoretical Model of UHF Propagation in Urban Environments," *IEEE Transactions on Antenas and Propagation*, Vol. 36, No. 12, pp. 1788–1796, 1988.

[17] K. Low, "Comparison of Urban Propagation Models with CW-Measurements," *IEEE Vehicular Technology Society 42nd VTS Conferenc:. Frontiers of Technology—From Pioneers to the 21st Century*, Vol. 2, pp. 936–942, 1992.

[18] S. R. Saunders and F. R. Bonar, "Explicit Multiple Building Diffraction Attenuation Function for Mobile Radio Wave Propagation," *Electronic Letters*, Vol. 27, No. 14, pp. 1276–1277, July 1991.

[19] S. R. Saunders and F. R. Bonar, "Prediction of Mobile Radio Wave Propagation over Buildings of Irregular Heights and Spacings," *IEEE Transactions on Antennas and Propagation*, Vol. 42, No. 2, pp. 137–144, 1994.

[20] M. J. Neve and G. B. Rowe, "Assessment of GTD for Mobile Radio Propagation Prediction," *Electronics Letters*, Vol. 29, No. 7, pp. 618–620, Apr. 1993

[21] Juan-Llacer and N. Cardona, "UTD Solution for the Multiple Building Diffraction Attenuation Function for Mobile Radiowave Propagation," *Electronics Letters*, Vol. 33, No. 1, pp. 92–93, Apr. 1997.

[22] L. Juan-Llacer, L. Ramos, and N. Cardona, "Application of Some Theoretical Models for Coverage Prediction in Macrocell Urban Environments," *IEEE Transactions on Vehicular Technology,* Vol. 48, No. 5, pp. 1463–1468, 1999.

[23] D. Har, A. M. Watson, and A. G. Chadney, "Comment on Diffraction Loss of Rooftop-to-Street in Cost 231–Walfich–Ikegami Model," *IEEE Transactions on Vehicular Technology,* Vol. 48, No. 5, pp. 1451–1452, 1999.

[24] T. S. Rappaport and L. B. Milstein, "Effect of Radio Propagation Path Loss on DS-CDMA Cellular Frequency Reuse Efficiency for the Reverse Channel," *IEEE Transactions on Vehicular Technology*, Vol. 41, No. 3, pp. 231–242, Aug. 1992.

[25] H. Xia, H. L. Bertoni, L. R Maciel, A. Lindsay-Stewart, and R. Rowe, "Radio Propagation Characteristics for Line-of-Sight Microcellular and Personal Communications," *IEEE Transactions on Antennas and Propagation*, Vol. 41, No. 10, pp. 1439–1447, Oct. 1993.

[26] M. J. Feuerstein, K. L Blackard, T. S. Rappaport, S. Y. Seidel, and H. H. Xia, "Path Loss, Delay Spread, and Outage Models as Functions of Antenna Height for Macrocellular System Design," *IEEE Transactions on Vehicular Technology*, Vol. 43, No. 3, pp. 487–498, Aug. 1994.

[27] N. Beaunstein, "Prediction of Cellular Characteristics for Various Urban Environments," *IEEE Antennas and Propagation Magazine*, Vol. 41, No. 6, pp. 135–145, 1999.

[28] S. Ichitsubo, T. Furuno, T. Taga, and R. Kawasaki, "Multipath Propagation Model for Line-of-Sight Street Microcells in Urban Area," *IEEE Transactions on Vehicular Technology,* Vol. 49, No. 2, pp. 422–427, 2000.

[29] T. S. Rappaport and S. Sandhu, "Radio-Wave Propagation for Emerging Wireless Personal-Communication Systems," *IEEE Antennas and Propagation Magazine*, Vol. 36, No. 5, pp. 14–24, Oct. 1994.

[30] A. A. M. Saleh and R. L. Valenzuela, "A Statistical Model for Indoor Multipath Propagation," *IEEE Journal on Selected Areas in Communications*, Vol. 5, No. 2, pp. 128–137, 1987.

[31] R. J. C. Bultitude, "Measurement Characterization and Modeling of Indoor 800/900 MHz Radio Channels for Digital Communications," *IEEE Communications Magazine*, Vol. 5, No. 6, pp. 5–12, 1987.

[32] F. C. Owen and C. D. Pundey, "In-Building Propagation at 900 MHz and 1650 MHz for Digital Cordless Telephone," *Proceedings of the 6th International Conference on Antennas and Propagation, ICAP'89*, Part 2, *Propagation*, pp. 276–281, 1989.

[33] P. Valch, B. Segal, J. Lebel, and T. Pavlasek, "Cross-Floor Signal Propagation inside a Contemporary Ferro-Concrete Building at 434, 864, and 1705 MHz," *IEEE Transactions on Antennas and Propagation*, Vol. 47, No. 7, pp. 1230–1232, 1999.

[34] S. E. Alexander, "Characterising Buildings for Propagation at 900 MHz," *Electronics Letters*, Vol. 19, No. 20, p. 860, Sept. 1983.

[35] S. Y. Seidel and T. S. Rappaport, "914 MHz Path Loss Prediction Models for Indoor Wireless Communications in Multifloored Buildings," *IEEE Transactions on Antennas and Propagation*, Vol. 40, pp. 207–217, 1992.

[36] T. S. Rappaport, "Characterization of UHF Multipath Radio Channels in Factory Buildings," *IEEE Transactions on Antennas and Propagation*, Vol. 37, No. 8, pp. 1058–1069, Aug. 1989.

[37] K. Pahlavan, R. Ganesh, and T. Hotaling, "Multipath Propagation Measurements on Manufacturing Floors at 910 MHz," *Electronics Letters*, Vol. 25, No. 3, pp. 225–227, Feb. 1989.

[38] D. A. Haand, "Indoor Wide Band Radio Wave Propagation and Models at 1.3 GHz and 4.0 GHz," *Electronics Letters*, Vol. 26, No. 21, pp. 1800–1802, Oct. 1990.

[39] Telesis Technologies Laboratory, *Experimental License Report to FCC*, Aug. 1991.

[40] D. M. J. Davasirvatham, "A Comparison of Time Delay Spread and Signal Level Measurements within Two Dissimilar Office Buildings," *IEEE Transactions on Antennas and Propagation*, Vol. 35, No. 3, pp. 319–324, Mar. 1987.

[41] K. W. Cheung, J. H. M. Sau, and R. D. Murch, "A New Empirical Model for Indoor Propagation Prediction," *IEEE Transactions on Vehicular Technology*, Vol. 47, No. 3, pp. 996–1001, Aug. 1998.

[42] W. Honcharenko, H. L. Bertoni, and J. Dailing, "Mechanisms Governing UHF Propagation on Single Floors in Modern Office Buildings," *IEEE Transactions on Antennas and Propagation*, Vol. 41, No. 4, pp. 496–504, 1992.

[43] S. Ruiz, Y. Samper, J. Perez, R. Agusti, and J. Olmos, "Software Tool for Optimising Indoor/Outdoor Coverage in a Construction Site," *Electronics Letters*, Vol. 34, No. 22, pp. 2100–2101, Oct. 1998.

[44] G. M. Whitman, K. S. Kim, and E. Niver, "A Theoretical Model for Radio Signal Attenuation inside Buildings," *IEEE Transactions on Vehicular Technology*, Vol. 44, No. 3, pp. 621–629, Aug. 1995.

[45] R. J. Luebbers, "Finite Conductivity Uniform GTD versus Knife Edge Diffraction in Prediction of Propagation Path Loss," *IEEE Transactions on Antennas and Propagation*, Vol. 32, No. 1, pp. 70–76, Jan. 1984.

[46] F. Ikegami, T. Takeuchi, and S. Yoshida, "Theoretical Prediction of Mean Field Strength for Urban Mobile Radio," *IEEE Transactions on Antennas and Propagation*, Vol. 39, No. 3, pp. 299–302, Mar. 1991.

[47] W. K. Tam and V. N. Tran, "Propagation Modeling for Indoor Wireless Communication," *Electronics and Communication Engineering Journal*, pp. 221–228, Oct. 1995.

[48] J. W. McKown and R. L. Hamilton, Jr., "Ray Tracing as a Design Tool for Radio Networks," *IEEE Network Magazine*, Vol. 5, pp. 27–30, Nov. 1991.

[49] S. Y. Tan and H. S. Tan, "Improved Three-Dimension Ray Tracing Technique for Microcellular Propagation," *Electronics Letters*, Vol. 31, No. 17, pp. 1503–1505, Aug. 1995.

[50] S. Y. Tan and H. S. Tan, "Propagation Model for Microcellular Communications Applied to Path Loss Measurements in Ottawa City Streets," *IEEE Transactions on Vehicular Technology*, Vol. 44, No. 2, pp. 313–317, May 1995.

[51] S. Y. Tan and H. S. Tan, "A Theory for Propagation Path-Loss Characteristics in a City-Street Grid," *IEEE Transactions on Electromagnetic Compatibility*, Vol. 37, No. 3, pp. 333 –342, Aug. 1995.

[52] M. G. Sanchez, L. de Haro, A. G. Pino, and M. Calvo, "Exhaustive Ray Tracing Algorithm for Microcellular Propagation Prediction Models," *Electronics Letters*, Vol. 32, No. 7, pp. 624–625, Mar. 1996.

[53] S. H. Chen and S. K. Jeng, "SBR Image Approach for Radio Wave Propagation in Tunnels with and without Traffic," *IEEE Transactions on Vehicular Technology*, Vol. 45, No. 3, pp. 570–578, Aug. 1996.

[54] S. H. Chen and S. K. Jeng, "An SBR/Image Approach for Radio Wave Propagation in Indoor Environments with Metallic Furniture," *IEEE Transactions on Antennas and Propagation*, Vol. 45, No. 1, pp. 98–106, Jan. 1997.

[55] F. Villanese, W. G. Scanlon, N. E. Evans, and E. Gambi, "Hybrid Image/Ray-Shooting UHF Radio Propagation Predictor for Populated Indoor Environments," *Electronics Letters*, Vol. 35, No. 21, pp. 1804–1805, Oct. 1999.

[56] M. C. Lawton and J. P. McGeehan, "The Application of a Deterministic Ray Launching Algorithm for the Prediction of Radio Channel Characteristics in Small-Cell Environments," *IEEE Transactions on Vehicular Technology*, Vol. 43, No. 4, pp. 955–969, Nov. 1994.

[57] U. Dersch and E. Zollinger, "Propagation Mechanisms in Microcell and Indoor Environments," *IEEE Transactions on Vehicular Technology*, Vol. 43, No. 4, pp. 1058–1066, Nov. 1994.

[58] K. Rizk, J. F. Wagen, and F. Gardiol, "Two-Dimensional Ray-Tracing Modeling for Propagation Prediction in Microcellular Environments,"

*IEEE Transactions on Vehicular Technology*, Vol. 46, No. 2, pp. 508–518, May 1997.

[59] G. M. Whitman, K. S. Kim, and E. A. Niver, "Theoretical Model for Radio Signal Attenuation Inside Buildings," *IEEE Transactions on Vehicular Technology*, Vol. 44, No. 3, pp. 621–629, Aug. 1995.

[60] J. H. Tarng and T. R. Liu, "Effective Models in Evaluating Radio Coverage on Single Floors of Multifloor Buildings," *IEEE Transactions on Vehicular Technology*, Vol. 48, No. 3, pp. 782–789, May 1999.

[61] S. C. Jan and S. K. Jeng, "A Novel Propagation Modeling for Microcellular Communications in Urban Environments," *IEEE Transactions on Vehicular Technology*, Vol. 46, No. 4, pp. 1021–1026, Nov. 1997.

[62] W. Zhang, "Fast Two-Dimensional Diffraction Modeling for Site-Specific Propagation Prediction in Urban Microcellular Environments," *IEEE Transactions on Vehicular Technology*, Vol. 49, No. 2, pp. 428–436, Mar. 2000.

[63] H. Mokhtari and P. Lazaridis, "Comparative Study of Lateral Profile Knife-Edge Diffraction and Ray Tracing Technique Using GTD in Urban Environment," *IEEE Transactions on Vehicular Technology*, Vol. 48, No. 1, pp. 255–261, Jan. 1999.

[64] S. C. Kim, B. J. Guarino, Jr., T. M. Willis III, V. Erceg, S. J. Fortune, R. A.Valenzuela, L. W. Thomas, J. Ling, and J. D. Moore, "Radio Propagation Measurements and Prediction Using Three-Dimensional Ray Tracing in Urban Environments at 908 MHz and 1.9 GHz," *IEEE Transactions on Vehicular Technology*, Vol. 48, No. 3, pp. 931–944, 1999.

[65] J. H. Tarng, W. R. Chang, and B. J. Hsu, "Three-Dimensional Modeling of 900-MHz and 2.44-GHz Radio Propagation in Corridors," *IEEE Transactions on Vehicular Technology*, Vol. 46, No. 2, pp. 519–527, May 1997.

[66] G. Liang and H. L. Bertoni, "A New Approach to 3-D Ray Tracing for Propagation Prediction in Cities," *IEEE Transactions on Antennas and Propagation*, Vol. 46, No. 6, pp. 853–863, June 1998.

[67] G. Durgin, N. Patwari, and T. S. Rappaport, "Improved 3D Ray Launching Method for Wireless Propagation Prediction," *Electronics Letters*, Vol. 33, No. 16, pp. 1412–1413, July 1997.

[68] G. E. Athanasiadou, A. R. Nix, and J. P. McGeehan, "A Microcellular Ray-Tracing Propagation Model and Evaluation of Its Narrow-Band and Wide-Band Predictions," *IEEE Journal on Selected Areas in Communications*, Vol. 18, No. 3, pp. 322–335, Mar. 2000.

[69] J. P. Rossi, J. C. Bic, A. J. Levy, Y. Gabillet, and M. Rosen, "A Ray Launching Method for Radio-Mobile Propagation in Urban Area," *Proceedings of the IEEE Antennas and Propogation Symposium*, London, Ontario, Canada, Vol. 3, pp. 1540–1543, 1991.

[70] W. M. O'Brien, E. M. Kenny, and P. J. Cullen, "An Efficient Implementation of a Three-Dimensional Microcell Propagation Tool for

Indoor and Outdoor Urban Environments," *IEEE Transactions on Vehicular Technology*, Vol. 49, No. 2, pp. 622–630, Mar. 2000.

[71] M. F. Catedra, J. Perez-Saez, F. de Adana, and O. Gutierrez, "Efficient Ray-Tracing Techniques for Three-Dimensional Analyses of Propagation in Mobile Communications: Application to Picocell and Microcell Scenarios," *IEEE Antennas and Propagation Magazine*, Vol. 40, No. 2, pp. 15–28, Apr. 1998.

[72] V. Erceg, S. J. Fortune, J. Ling, A. J. Rustako, Jr., and R. A. Valenzuela, "Comparisons of a Computer-Based Propagation Prediction Tool with Experimental Data Collected in Urban Microcellular Environments," *IEEE Journal on Selected Areas in Communications*, Vol. 15, No. 4, pp. 677–684, May 1997.

[73] J. W. Schuster and R. J. Luebbers, "Comparison of GTD and FDTD Predictions for UHF Radio Wave Propagation in a Simple Outdoor Urban Environment," *IEEE Antennas and Propagation Society International Symposium, 1997 Digest*, Vol. 3, pp. 2022–2025, 1997.

[74] G. D. Kondylis, F. DeFlaviis, G. J. Pottie, and Y. Rahmat-Samii, "Indoor Channel Characterization for Wireless Communications Using Reduced Finite Difference Time Domain," *Proceedings of the IEEE Vehicular Technology Conference, 1999*, Vol. 3, pp. 1402–1406, 1999.

[75] A. Lauer, I. Wolff, A. Bahr, J. Pamp, and J. Kunisch, "Multi-Mode FDTD Simulations of Indoor Propagation Including Antenna Properties," in *Proceedings of the IEEE 45th Vehicular Technology Conference*, Chicago, pp. 454–458, 1995.

[76] W. Ying, S. Safavi-Naini, and S. K. Chaudhuri, "A Hybrid Technique Based on Combining Ray Tracing and FDTD Methods for Site-Specific Modeling of Indoor Radio Wave Propagation," *IEEE Transactions on Antennas and Propagation*, Vol. 48, No. 5, pp. 743–754, May 2000.

[77] C. Yang, B. Wu, and C. Ko, "A Ray-Tracing Method for Modeling Indoor Wave Propagation and Penetration," *IEEE Transactions on Antennas and Propagation*, Vol. 46, No. 6, pp. 907–919, June 1998.

[78] B. De Backer, H. Borjeson, F. Olyslager, and D. De Zutter, "The Study of Wave-Propagation through a Windowed Wall at 1.8 GHz," *Proceedings of the IEEE 46th Vehicular Technology Conference: Mobile Technology for the Human Race*, Vol. 1, pp. 165–169, 1996.

[79] C. Yang and B. Wu, "Simulations and Measurements for Indoor Wave Propagation Through Periodic Structures," *Proceedings of the IEEE International Symposium Antennas and Propagation Society*, Vol. 1, pp. 384–387, 1999.

[80] Z. Sandor, L. Nagy, Z. Szabo, and T. Csaba, "3D Ray Launching and Moment Method for Indoor Propagation Purposes," *Proceedings of the 8th IEEE International Symposium on Personal, Indoor and Mobile Radio Communications: Waves of the Year 2000*, PIMRC '97, Vol. 1, pp. 130–134, 1997.

[81] A. Neskovic and D. Paumovic, "Indoor Electric Field Level Prediction Model Based on the Artificial Neural Networks," *IEEE Communications Letters*, Vol. 4, No. 6, pp. 190–192, 2000.

[82] K. E. Stocker, B. E. Gschwendtner, and F. M. Landstorfer, "Neural Network Approach to Prediction of Terrestrial Wave Propagation for Mobile Radio," *IEE Proceedings H: Microwaves, Antennas and Propagation*, Vol. 140, No. 4, pp. 315–320, Aug. 1993.

[83] P. Chang and W. Yang, "Environment-Adaptation Mobile Radio Propagation Prediction Using Radial Basis Function Neural Networks," *IEEE Transactions on Vehicular Technology*, Vol. 46, No. 1, pp. 155–160, Feb. 1997.

[84] A. A. Zaporozhets, "Application of Vector Parabolic Equation Method to Urban Radiowave Propagation Problems," *IEE Proceedings H: Microwaves, Antennas and Propagation*, Vol. 146, No. 4, pp. 253–256, Aug. 1999.

[85] C. Brennan and P. J. Cullen, "Application of the Fast Far-field Approximation to the Computation of UHF Pathloss over Irregular Terrain," *IEEE Transactions on Antennas and Propagation*, Vol. 46, No. 6, pp. 881–890, June 1998.

[86] R. Mazar and A. Bronshtein, "Propagation Model of a City Street for Personal and Microcellular Communications," *Electronics Letters*, Vol. 33, No. 1, pp. 91–92, Jan. 1997.

[87] N. Blaunstein, "Average Field Attenuation in the Street Waveguide," *IEEE Transactions on Antennas and Propagation*, Vol. 46, No. 12, pp. 1782–1789, Dec.1998.

[88] B. Chopard, P. O. Luthi, and J. F. Wagen, "Lattice Boltzmann Method for Wave Propagation in Urban Microcells," *IEE Proceedings: Antennas and Propagation*, Vol. 144, No. 4, pp. 251–255, Aug. 1997.

[89] L. J. Greenstein, D. G. Michelson, and V. Erceg, "Moment-Method Estimation of the Ricean K-Factor," *IEEE Communications Letters*, Vol. 3, No. 6, pp. 175–176, June 1999.

[90] V. Fung, T. S. Rappaport, and B. Thomas, "Bit Error Simulation for pi/4 DQPSK Mobile Radio Communications Using Two-Ray and Measurement-Based Impulse Response Models," *IEEE Journal on Selected Areas in Communications*, Vol. 11, No. 3, pp. 393–405, Apr. 1993.

[91] C. C. Hess, *Handbook of Land-Mobile Radio System Coverage*, Artech House, Norwood, MA.

[92] A. Safak, "Statistical Analysis of the Power Sum of Multiple Correlated Lognormal_Components," *IEEE Transactions on Vehicular Technology*, Vol. 42, No. 1, pp. 58–61, Feb. 1993.

[93] H. Suzuki, "A Statistical Model for Urban Radio Propagation," *IEEE Transactions on Communications*, Vol. 25, pp. 673–680, 1977.

[94] A. Krantzik and D. Wolf, "Analysis of a Modified Suzuki Fading Channel Model," *Proceedings of the 1989 International Conference on Acoustics,*

*Speech, and Signal Processing,* 1989 ICASSP-89, Vol. 4, pp. 2250–2253, 1989.

[95] M. Patzold, U. Killat, and F. Laue, "A Deterministic Digital Simulation Model for Suzuki Processes with Application to a Shadowed Rayleigh Land Mobile Radio Channel," *IEEE Transactions on Vehicular Technology*, Vol. 45, No. 2, pp. 318–331, May 1996.

[96] IEEE Vehicular Technology Society Committee on Radio Propagation, "Coverage Prediction for Mobile Radio Systems Operating in the 800/900 MHz Frequency Range," *IEEE Transactions on Vehicular Technology*, Vol. 37, No. 1, pp. 3–72, Feb. 1988.

[97] K. Yip and T. Ng, "A Simulation Model for Nakagami-m Fading Channels, $m > 1$," *IEEE Transactions on Communications*, Vol. 48, No. 2, pp. 214–221, Feb. 2000.

[98] F. Vatalaro, "Generalized Rice-Lognormal Channel Model for Wireless Communications," *Electronics Letters*, Vol. 31, No. 22 , pp. 1899–1900, Oct. 1995.

[99] Y. Karasawa and H. Iwai, "Modeling of Signal Envelope Correlation of Line-of-Sight Fading with Applications to Frequency Correlation Analysis," *IEEE Transactions on Communications*, Vol. 42 No. 6, pp. 2201–2203, June 1994.

[100] T. T. Tjhung and C. C. Chai, "Fade Statistics in Nakagami-Lognormal Channels," *IEEE Transactions on Communications*, Vol. 47, No. 12, pp. 1769–1772, Dec. 1999.

[101] A. Abdi and M. Kaveh, "K Distribution: An Appropriate Substitute for Rayleigh-Lognormal Distribution in Fading-Shadowing Wireless Channels," *Electronics Letters*, Vol. 34, No. 9, pp. 851–852, Apr. 1998.

[102] G. E. Corazza and F. Vatalaro, "A Statistical Model for Land Mobile, Satellite Channels and Its Application to Nongeostationary Orbit Systems," *IEEE Transactions on Vehicular Technology*, Vol. 43, pp. 738–741, Aug. 1994.

[103] P. G. Babalis and C. N. Capsalis, "Impact of the Combined Slow and Fast Fading Channel Characteristics on the Symbol Error Probability for Multipath Dispersionless Channel Characterized by a Small Number of Dominant Paths," *IEEE Transactions on Communications*, Vol. 47, No. 5, pp. 653–657, May 1999.

[104] D. S. Polydorou and C. N. Capsalis, "A New Theoretical Model for the Prediction of Rapid Fading Variations in Indoor Environment," *IEEE Transactions on Vehicular Technology*, Vol. 46, pp. 748–755, Aug. 1997.

[105] R. J. C. Bultitude, P. Melancon, H. Zaghloul, G. Morrison, and M. Prokki, "The Dependence of Indoor Radio Channel Multipath Characteristics of Transmit/Receiver Ranges," *IEEE Journal on Selected Areas in Communications*, Vol. 11, No. 7, pp. 979–990, Sept. 1993.

[106] D. M. J. Devasirvatham, R. R. Murray, and C. Banerjee, "Time Delay Spread Measurements at 850 MHz and 1.7 GHz inside a Metropolitan Office Building," *Electronics Letters*, Vol. 25, No. 3, pp. 194–196, Feb. 1989.

[107] H. Zaghbul, M. Fattouche, G. Morrison, and D. Tholl, "Comparison of Indoor Propagation Channel Characteristics at Different Frequencies," *Electronics Letters*, Vol. 27, No. 22, pp. 2077–2079, Oct. 1991.

[108] G. J. M. Janssen, P. A. Stigter, and R. Prasad, "Wideband Indoor Channel Measurements and BER Analysis of Frequency Selective Multipath Channels at 2.4, 4.75, and 11.5 GHz," *IEEE Transactions on Communications*, Vol. 44, No. 10, pp. 1272–1288, Oct. 1996.

[109] K. Pahlavan, R. Ganesh, and T. Hotaling, "Multipath Propagation Measurements on Manufacturing Floors at 910 MHz," *Electronics Letters*, Vol. 25, No. 3, pp. 225–227, Feb. 1989.

[110] D. A. Hawbaker and T. S. Rappaport, "Indoor Wideband Radiowave Propagation Measurements at 1.3 GHz and 4.0 GHz," *Electronics Letters*, Vol. 26, No. 21, pp. 1800–1802, Oct. 1990.

[111] L. Talbi and G. Y. Delisle, "Experimental Characterization of EHF Multipath Indoor Radio Channels," *IEEE Journal on Selected Areas in Communications*, Vol. 14, No. 3, pp. 431–440, Apr. 1996.

[112] R. J. C. Bultitude and G. K. Bedal, "Propagation Characteristics on Microcellular Urban Mobile Radio Channels at 910 MHz," *IEEE Journal on Selected Areas in Communications*, Vol. 7, No. 1, pp. 31–39, Jan. 1989.

[113] R. J. C. Bultitude, R. F. Hahn, and R. J. Davies, "Propagation Considerations for the Design of an Indoor Broad-Band Communications System at EHF," *IEEE Transactions on Vehicular Technology*, Vol. 47, No. 1, pp. 235–245, Feb. 1998.

[114] S. Ichitsubo, T. Furuno, T. Taga, and R. Kawasaki, "Multipath Propagation Model for Line-of-Sight Street Microcells in Urban Area," *IEEE Transactions on Vehicular Technology*, Vol. 49, pp. 422–427, Mar. 2000.

[115] S. C. Kim, H. L. Bertoni and M. Stern, "Pulse Propagation Characteristics at 2.4 GHz inside Buildings," *IEEE Transactions on Vehicular Technology*, Vol. 45, No. 3, pp. 579–592, Aug. 1996.

[116] T. R. Liu and J. H. Tarng, "Modeling and Measurement of 2.44 GHz Radio Out-Of-Sight Propagation on Single Floors," *Microwave and Optical Technology Letters*, Vol. 14, No. 1 pp. 56–59, Jan. 1997.

[117] R. Ganesh and K. Pahlavan, "Statistics of Short Time and Spatial Variations Measured in Wideband Indoor Radio Channels," *IEE Proceedings H: Antennas and Propagation*, Vol. 140, No. 4, pp. 297–302, Aug. 1993.

[118] M. C. Lawton and J. P. McGeehan, "The Application of a Deterministic Ray Launching Algorithm for the Prediction of Radio Channel Characteristics in Small-Cell Environments," *IEEE Transactions on Vehicular Technology*, Vol. 43, No. 4, pp. 955–969, Nov. 1994.

[119] H. Hashemi, "Impulse Response Modeling of Indoor Radio Propagation Channels," *IEEE Journal on Selected Areas in Communications*, Vol. 11, No. 7, pp.967–978, Sept. 1993.

[120] S. Y. Seidel, T. S. Rappaport, S. Jain, M. L. Lord, and R. Singh, "Path Loss, Scattering and Multipath Delay Statistics in Four European Cities for Digital Cellular and Microcellular Radiotelephone," *IEEE Transactions on Vehicular Technology*, Vol. 40, No. 4, pp. 721–730, Nov. 1991.

[121] T. S. Rappaport and S. Y. Seidel, "900 MHz Multipath Propagation Measurements in Four States' Cities," *Electronics Letters*, Vol. 25, No. 15, pp. 956–958, July 1989.

[122] T. Taga, T. Furuno, and K. Suwa, "Channel Modeling for 2-GHz-band Urban Line-of-Sight Street Microcells," *IEEE Transactions on Vehicular Technology*, Vol. 48, No. 1, pp. 262–272, Jan. 1999.

[123] H. Son and N. Myung, "A Deterministic Ray Tube Method for Microcellular Wave Propagation Prediction Model," *IEEE Transactions on Antennas and Propagation*, Vol. 47, No. 8, pp. 1344–1350, Aug. 1999.

[124] L. J. Greenstein, V. Erceg, Y. S. Yeh, and M. V. Clark, "A New Path-Gain/Delay-Spread Propagation Model for Digital Cellular Channels," *IEEE Transactions on Vehicular Technology*, Vol. 46, No. 2, pp. 477–485, May 1997.

[125] R. Ganesh and K. Pahlavan, "Statistical Modelling and Computer Simulation of Indoor Radio Channel," *IEE Proceedings I: Communications, Speech and Vision*, Vol. 138, No. 3, pp. 153–161, June 1991.

[126] R. A. Valenzula, O. Landron, and D. L. Jacobs, "Estimating Local Mean Signal Strength of Indoor Multipath Propagation," *IEEE Transactions on Vehicular Technology,* Vol. 46, No. 1, pp. 203–212, Feb. 1997.

[127] G. E. Athanasiadou, A. R. Nix, and J. P. McGeehan, "A Microcellular Ray-Tracing Propagation Model and Evaluation of Its Narrow-Band and Wide-Band Predictions," *IEEE Journal on Selected Areas in Communications*, Vol. 18, No. 3, pp. 322–335, Mar. 2000.

[128] Z. Ji, B. H. Li, H. X. Wang, H. Y. Chen, and Y. G. Zhou, "An Improved Ray-Tracing Propagation Model for Predicting Path Loss on Single Floors," *Microwave and Optical Technology Letters*, Vol. 22, No. 1, pp. 39–41, 1999.

[129] W. K. Tam and V. N. Tran, "Multi-ray Propagation Model for Indoor Wireless Communications," *Electronics Letters*, Vol. 32, No. 2, pp. 135–137, 1996.

[130] K. R. Chang and H. T. Kim, "Improvement of the Computation Efficiency for a Ray-Launching Model," *IEE Proeedings: Microwave Antennas and Propagation*, Vol. 145, No. 4, pp. 303–308, 1997.

[131] T. B. Gibson and D. C. Jenn, "Prediction and Measurement of Wall Insertion Loss," *IEEE Transactions on Antennas and Propagation*, Vol. 47, No. 1, pp. 55–57, 1999.

[132] J. A. Kong, *Theory of Electromagnetic Waves*, John Wiley, New York, 1975.

[133] G. Ghobadi, P. R. Shepherd, and S. R. Pennock, "2D Ray-Tracing Model for Indoor Radio Propagation at Millimeter Frequencies, and the Study of

Diversity Techniques," *IEE Proceedings: Microwave Antennas and Propagation*, Vol. 145, No. 4, pp. 349–353, 1998.

[134] W. Honcharenko and H. L. Bertoni, "Transmission and Reflection Characteristics at Concrete Block Walls in the UHF Bands Proposal for Future PCs," *IEEE Transactions on Antennas and Propagation*, Vol. 42, No. 2, pp. 232–239, Feb. 1994.

[135] C. L. Holloway and P. L. Perini, "Analysis of Composite Walls and Their Effects on Short-Path Propagation Modeling," *IEEE Transactions on Vehicular Technology*, Vol. 46, No. 3, pp. 730–738, Aug. 1997.

[136] Z. Ji, B. H. Li, H. X. Wang, H. Y. Chen, and T. K. Sarkar, "Efficient Ray-Tracing Methods for Propagation Prediction for Indoor Wireless Communications," *IEEE Antennas and Propagation Magazine*, Vol. 43, No. 2, pp. 41–49, Apr. 2001.

[137] Z. Ji, T. K. Sarkar, and B. H. Li, "Analysis of the Effects of Walls on Indoor Wave Propagation Using the FDTD Method," *Microwave and Optical Technology Letters*, Vol. 29, No. 1, pp. 19–21, 2001.

[138] C. A. Zelley and C. C. Constantinou, "A Three-Dimensional Parabolic Equation Applied to VHF/UHF Propagation over Irregular Terrain," *IEEE Transactions on Antennas and Propagation*, Vol. 47, No. 10, pp. 1586–1596, 1999.

[139] D. J. Donohue and J. R. Kuttler, "Propagation Modeling over Terrain Using the Parabolic Wave Equation," *IEEE Transactions on Antennas and Propagation*, Vol. 48, No. 2 , pp. 260–277, 2000.

[140] Y. P. Zhang, Y. Hwang and J. D. Parsons, "UHF Radio Propagation Characteristics in Straight Open-Groove Structures," *IEEE Transactions on Vehicular Technology*, Vol. 48, No. 1, pp. 249–254, 1999.

[141] D. Har, H. H. Xia, and H. L. Bertoni, "Path-Loss Prediction Model for Microcells," *IEEE Transactions on Vehicular Technology*, Vol. 48, No. 5, pp. 1453–1462, 1999.

[142] H. L. Bertoni, W. Honcharenko, L. R. Macel, and H. H. Xia, "UHF Propagation Prediction for Wireless Personal Communications," *Proceedings of the IEEE*, Vol. 82, No. 9, pp. 1333–1359, 1994.

[143] D. Ullmo and H. U. Baranger, "Wireless Propagation in Buildings: A Statistical Scattering Approach," *IEEE Transactions on Vehicular Technology*, Vol. 48, No. 3, pp. 947–955, 1999.

[144] S. Kozono and A. Taguchi, "Mobile Propagation Loss and Delay Spread Characteristics with a Low Base Station Antenna on an Urban Road," *IEEE Transactions on Vehicular Technology*, Vol. 42, No. 1, pp. 103–109, 1993.

[145] S. Obayashi and J. Zander, "A Body-shadowing Model for Indoor Radio Communication Environments," *IEEE Transactions on Antennas and Propagation*, Vol. 46, No. 6 , pp. 920–927, 1998.

[146] F. Babich and G. Lombardi, "Statistical Analysis and Characterization of the Indoor Propagation Channel," *IEEE Transactions on Communications*, Vol. 48, No. 3, pp. 455–464, 2000.

[147] H. Hashemi and D. Tholl, "Statistical Modeling and Simulation of the RMS Delay Spread of Indoor Radio Propagation Channels," *IEEE Transactions on Vehicular Technology*, Vol. 43, No. 1, pp. 110–120, 1993.

[148] J. A. Wepman, J. R. Hoffman, and L. H. Loew, "Analysis of Impulse Response Measurements for PCS Channel Modelling Applications," *IEEE Transactions on Vehicular Technology*, Vol. 44, No. 3, pp. 613–620, 1995.

[149] C. L. Holloway, M. G. Cotton, and P. McKenna, "A Model for Predicting the Power Delay Profile Characteristics inside a Room," *IEEE Transactions on Vehicular Technology*, Vol. 48, No. 4, pp. 1110–1120, 1999.

[150] P. E. Driessen, "Prediction of Multipath Delay Profiles in Mountainous Terrain," *IEEE Journal on Selected Areas in Communications*, Vol. 18, No. 3, pp. 336–346, 2000.

[151] Y. Li, "A Theoretical Formulation for the Distribution Density of Multipath Delay Spread in a Land Mobile Radio Environment," *IEEE Transactions on Vehicular Technology*, Vol. 43, No. 2, pp. 379–388, 1994.